# Neutron Stars – Thermal Emitters

**Alexander Y. Potekhin** · **Andrea De Luca** ·
**José A. Pons**

**Abstract** Confronting theoretical models with observations of thermal radiation emitted by neutron stars is one of the most important ways to understand the properties of both, superdense matter in the interiors of the neutron stars and dense magnetized plasmas in their outer layers. Here we review the theory of thermal emission from the surface layers of strongly magnetized neutron stars, and the main properties of the observational data. In particular, we focus on the nearby sources for which a clear thermal component has been detected, without being contaminated by other emission processes (magnetosphere, accretion, nebulae). We also discuss the applications of the modern theoretical models of the formation of spectra of strongly magnetized neutron stars to the observed thermally emitting objects.

**Keywords** neutron stars · magnetic fields · thermal emission · stellar atmospheres

## 1 Introduction

One of the first expectations of neutron-star (NS) astrophysics, dating back to the epoch when such sources where theoretically proposed, is the possibility to detect thermal radiation from their hot (millions of K) surfaces (Zwicky 1938). Observation

A.Y. Potekhin
Ioffe Institute, Politekhnicheskaya 26, 194021 Saint Petersburg, Russia;
Central Astronomical Observatory at Pulkovo, Pulkovskoe Shosse 65, 196140 Saint Petersburg, Russia
E-mail: palex@astro.ioffe.ru

A. De Luca
INAF – Istituto di Astrofisica Spaziale e Fisica Cosmica Milano, via E. Bassini 15, 20133, Milano, Italy;
INFN – Istituto Nazionale di Fisica Nucleare, sezione di Pavia, via A. Bassi 6, 27100, Pavia, Italy
E-mail: deluca@iasf-milano.inaf.it

J.A. Pons
Departament de Física Aplicada, Universitat d'Alacant, Ap. Correus 99, E-03080 Alacant, Spain
E-mail: jose.pons@ua.es

of the first sources of cosmic X-rays in the Early Sixties suggested that NSs could indeed be detected, which added impetus to theoretical work as well as to modeling of expected NS observational properties. The crucial point, attracting a lot of interest in the astrophysical community, was that the study of NS cooling could constrain the physical properties of superdense matter in the interiors of the NSs (Bahcall and Wolf 1965), under conditions that cannot be studied in terrestrial laboratories. Discovery of NSs as radio pulsars (Hewish et al. 1968) further boosted NS cooling studies as well as observational efforts. However, the first detection of thermal radiation from the surface of INSs (Cheng and Helfand 1983; Brinkmann and Ögelman 1987) had to wait the launch of focusing X-ray telescopes HEAO2/*Einstein* (1978–1981) and *EXOSAT* (1983–1986), which allowed for a dramatic leap forward in sensitivity to faint point X-ray sources.

Our understanding of the physics of NSs dramatically improved in the last decades. Thanks to multiwavelength observations (with an important role played by X-ray observations), we have discovered with much surprise that not all Isolated NSs (INSs) behave as radio pulsars, but that there exist a rich diversity of INS classes, including Rotation-Powered Pulsars, Rotating Radio Transients, Anomalous X-ray Pulsars, Soft Gamma Repeaters, Central Compact Objects in supernova remnants, and the Magnificent Seven thermally emitting NSs (see the next section). It is now commonly accepted that magnetic fields plays an important role in shaping the electromagnetic emission properties of INSs, e.g. mediating the conversion of their rotational energy into radiation (as in rotation-powered sources), or directly acting as the energy reservoir for most of the INS luminosity (as in magnetars).

One of the main challenges is to disentangle different emission components, overlapping in the X-ray energy range. After discriminating thermal emission, a detailed study of the thermal spectra can yield precious information about the NS surface temperature distribution, the properties of dense magnetized plasmas in their envelopes and atmospheres, as well as set constraints on the equation of state of the ultradense matter in the NS cores.

Besides INSs, some NSs with observed thermal spectra also reside in binary systems. In low-mass X-ray binary systems (LMXBs), a NS accretes matter from a less massive star (a Main Sequence star or a white dwarf), alternating periods of intense accretion and periods of quiescence. When accretion stops and the residual heat diffuses out from the crust, X-ray radiation comes from the heated NS surface (Brown et al. 1998). During the last decade, such quiescent sources (qLMXBs) yield ever increasing amount of valuable information on the NSs. Their spectra are successfully interpreted with models of NS atmospheres (see Potekhin 2014, for a discussion and references). Another class of NSs in binaries with thermal spectra are X-ray bursters – accreting NSs in close binary systems, which produce X-ray bursts with intervals from hours to days (see, e.g. Strohmayer and Bildsten 2006, for a review). During intervals between the bursts, a burster's atmosphere does not essentially differ from an atmosphere of a cooling NS. In such periods, the bulk of the observed X-ray radiation arises from transformation of gravitational energy of the accreting matter into thermal energy. Some of the bursts (so-called long bursts, which last over a minute) occur during periods when the accretion rate is low enough for the lumi-

nosity not to exceed a few percent of the Eddington limit. In this cases, a thermal atmospheric spectrum can be observed (e.g., Suleimanov et al. 2011).

As we will see, the number of known NSs with an unambiguously identified thermal component in the spectrum is not large, but it steadily increases. Some of them can be understood with models of nonmagnetic atmospheres, whereas others are believed to be endowed with strong magnetic fields, which must be taken into account. After the seminal work of Romani (1987), the nonmagnetic neutron-star atmospheres have been studied in many works (see Zavlin 2009 for a review). Databases of neutron-star hydrogen atmosphere model spectra have been published (Zavlin et al. 1996; Gänsicke et al. 2002; Heinke et al. 2006),[1] and a computer code for their calculation has been released (Haakonsen et al. 2012). A database of carbon atmosphere model spectra has been also published recently (Suleimanov et al. 2014).[2] Model spectra were calculated for neutron-star atmospheres composed of different chemical elements from H to Fe (e.g., Rajagopal and Romani 1996; Pons et al. 2002; Heinke et al. 2006; Ho and Heinke 2009) and mixtures of different elements (Gänsicke et al. 2002; Pons et al. 2002). In general, the thermal spectra of NSs in binaries (e.g., bursters and qLMXBs mentioned above) are interpreted with theoretical models without magnetic fields. Thermal components of spectra of several millisecond pulsars (e.g., PSR J0437−4715, Bogdanov 2013 and some thermally emitting INSs (e.g., the source in Cassiopeia A, Ho and Heinke 2009) have also been interpreted with the nonmagnetic atmosphere models. In this paper, however, we will not consider the nonmagnetic models (see Potekhin 2014 for a more general review, which includes a discussion of both the nonmagnetic and magnetic cases), but instead we will focus on models of thermal spectra of the INSs that are significantly affected by strong magnetic fields.

The paper is organized as follows. In Sect. 2 we give account of the different classes of INSs. In Sect. 3 we list INSs with confirmed thermal emission and give a summary of their main characteristics. In Sect. 4 we consider the definitions and concepts that are important for the theory of formation of thermal spectra of NSs with strong magnetic fields. The latter theory is described in Sect. 5. Section 6 is devoted to the theory of a magnetized condensed surface as an alternative to gaseous NS atmospheres. In Sect. 7 we describe transformation of the local spectra into the spectra seen by a distant observer. Examples of interpretation of observed spectra with the use of theoretical models of partially ionized, strongly magnetized NS atmospheres are considered in Sect. 8. In sect. 9, we give brief conclusions. In the Appendix we briefly describe the effects of thermal motion of atoms in a strong magnetic field on the atomic quantum-mechanical characteristics and on the ionization equilibrium of plasmas, that underlie calculations of the opacities for the strongly magnetized NS atmospheres.

---

[1]  Models NSA, NSAGRAV, and NSATMOS in the database *XSPEC* (Arnaud 1996).

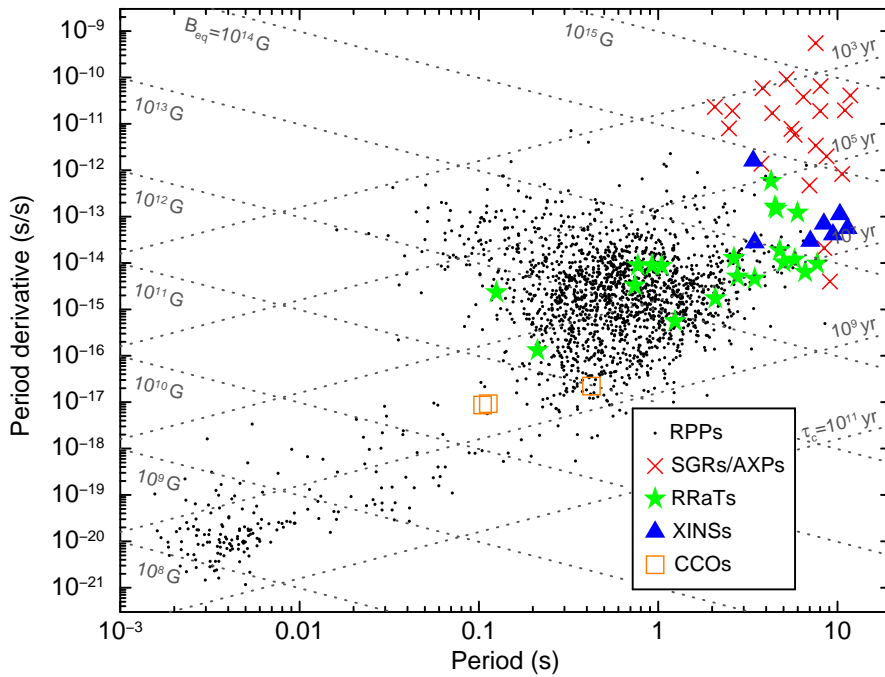[2]  Model CARBATM in the database *XSPEC* (Arnaud 1996).

**Fig. 1** $P - \dot{P}$ diagram for the $\sim 2300$ currently known neutron stars with measured $P$ and $\dot{P}$. Different classes are marked with different symbols. Lines showing constant $\dot{E}_{\rm rot}$ as well as constant inferred surface dipolar magnetic field are superimposed.

## 2 The families of Isolated Neutron Stars

A short account of the main properties of the different classes of INSs, with a focus on their emission in the X-ray range, is useful to set the context for the observational panorama of thermal emitters.

- **Rotation-Powered Pulsars (RPPs)**. This is the class of INSs with the largest observational database, more than 2,200 sources being known[3], mostly from radio surveys. A large population of radio-silent RPPs is also emerging, thanks to gamma-ray observations by the Fermi mission (see Abdo et al. 2013, and references therein).

Rotation of a magnetized INS induces electric fields which accelerate particles in the magnetosphere surrounding the star, initiating electromagnetic cascades. This mechanism produces synchrotron and curvature radiation along a peculiar beaming pattern, ultimately related to the magnetic field configuration, at the expense of the dissipation of the NS rotational energy (see Harding and Lai 2006, for a review). Because of such rotation-powered emission (see also Gwinn et al., this volume), RPPs are typically observed as pulsating sources from radio wavelengths[4] to very high en-

---

[3] See e.g. the ATNF pulsar database at http://www.atnf.csiro.au/research/pulsar/psrcat/ (Manchester et al. 2005)

[4] Indeed, their discovery as radio pulsars was the first observational evidence for the existence of NSs

ergy gamma-rays – the spin-down luminosity $\dot{E}_{rot} = 4\pi^2 I \dot{P} P^{-3}$ (where $I \sim 10^{45}$ g cm$^2$ is the NS moment of inertia) being indeed much larger than the inferred electromagnetic luminosities. However, as a matter of fact, most of the spin-down luminosity is carried away by a relativistic particle wind which, interacting with the surrounding medium, powers bright pulsar wind nebulae, seen as diffuse structures in the radio, X-ray, and gamma-ray energy ranges.

In this picture, assuming the observed $\dot{E}_{rot}$ to be due to magnetic dipole radiation yields an estimate of the surface dipole field at the magnetic equator of the star $B_{eq} = 3.2 \times 10^{19} (P\dot{P})^{1/2}$ G, as well as an estimate of the NS age $\tau_c = P/(2\dot{P})$, which is called characteristic age. The first estimate assumes $\sqrt{I_{45}}/(R_6^3 \sin\alpha) = 1$, where $I_{45} = I/10^{45}$ g cm$^2$, $R_6$ is the stellar radius $R$ in units of $10^6$ cm, and $\alpha$ is the angle between the magnetic and rotational axes. More realistic calculations give similar relations between $B$ and $P\dot{P}$ (Spitkovsky 2006; Beskin et al. 2013). The second estimate assumes a birth period much shorter than the current period $P$, as well as a non-variable magnetic field. As can be seen in Figure 1, the bulk of RPPs have $P$ in the $0.1 - 1$ s range and $B_{eq} \sim 10^{12}$ G. The separate subclass of Millisecond Pulsars (MSPs), accounting for $\sim 10\%$ of the RPP sample, is supposed to include very old NSs with a different evolutionary history, having experienced accretion in a long-lived binary system which eventually spun-up the NSs to $P \sim$ a few ms and quenched their magnetic field to $10^8 - 10^9$ G. For this reason MSPs are also called recycled pulsars (Bisnovatyi-Kogan 2006, and references therein).

More than 120 RPPs have been detected in the soft X-ray energy range (see, e.g., Marelli et al. 2011; Abdo et al. 2013), and several of them display thermal emission from their hot surfaces in addition to the rotation-powered emission. While a thermal component related to the NS cooling is apparent in a few sources, an additional component with a higher temperature and a smaller emitting area can also be observed (De Luca et al. 2005), probably related to re-heating of the magnetic polar caps by bombardment of magnetospheric particles. We note that RPPs with the largest inferred magnetic fields ($B_{eq} \sim 10^{13} - 10^{14}$ G) are often considered as a separate, "High-$B$" class, (HB, see Ng and Kaspi 2011 for a review). HB RPPs show some evidence for a larger thermal luminosity when compared to RPPs of similar ages and can be the link between magnetars and RPPs, with magnetic field decay playing an important role for their thermal evolution (Aguilera et al. 2008; Pons et al. 2009). At least in one case (PSR J1846−0258, Gavriil et al. 2008), a peculiar time variability, reminiscent of the behaviour of the anomalous X-ray pulsars (see below), has been seen in a HB RPP.

• **Rotating Radio Transients (RRaTs)**. Discovered as sources of repeated, bright, short ($\sim 1$ ms) radio bursts occurring at integral multiples of an underlying periodicity, RRaTs were initially considered as a new class of INSs (McLaughlin et al. 2006). High time resolution radio surveys are unveiling new RRaTs (about 70 are currently known – see Burke-Spolaor 2013 for a recent review).

It has been observed that RRaTs, as a class, have a larger magnetic field with respect to the bulk of RPPs, which prompted speculations about possible relationships of such sources with magnetars (or with HB RPPs, or with the Magnificent Seven NSs considered below). Interestingly enough, the most active RRaT (PSR J1819−1458) – the only source of its class being detected in soft X-rays – has an X-ray phenomenol-

ogy (as well as a position in the $P - \dot{P}$ plane) fully similar to the one of the Magnificent Seven, with a pulsed thermal-like emission and a broad spectral absorption feature superimposed to the continuum (Miller et al. 2011). In any case, it is currently believed that RRaTs are not substantially physically different from RPPs – which also show time variability of the radio pulses – RRaTs have just a somewhat extreme temporal behaviour.

• **Soft Gamma Repeaters (SGRs)** and **Anomalous X-ray Pulsars (AXPs)**. About two dozen such sources are known (Olausen and Kaspi 2014). Originally thought to form two different classes of objects, they were later shown to form a single SGR/AXP class (Gavriil et al. 2002). Detailed reviews of their phenomenology and physics are included in other chapters of this volume; see also Mereghetti (2008, 2013); Turolla and Esposito (2013).

The period of SGR/AXPs (in the $2 - 12$ s range) is much longer than the one of the bulk of RPPs; their period derivative (showing peculiar time variability) is also very large, corresponding to dipole magnetic fields of the order of $B \sim 10^{14} - 10^{15}$ G (see Figure 1).

These objects show a very complex high energy phenomenology. This includes a persistent, pulsed soft X-ray component (often with a transient behavior), dominated by thermal-like emission, typically with a luminosity largely exceeding the spin-down luminosity. Moreover, SGR/AXPs display a spectacular flaring emission component (see Rea and Esposito 2011, for a review), best seen from a few keV to a few hundreds keV. They are typically radio silent, although very bright radio pulses have been observed from a few sources.

SGR/AXPs are generally believed to be magnetars (see the review by Olausen and Kaspi 2014), i.e. NSs ultimately powered by the decay of their magnetic field (Duncan and Thompson 1992).[5] The magnetic field of magnetars is supposed to be much more intense than for other classes of INSs and to have a peculiar topology.

• **Central Compact Objects (CCOs)**. This class includes a dozen of point sources, lying close to the center of young ($0.3 - 10$ kyr) Supernova Remnants, discovered in the soft X-ray band and supposed to be young INSs (De Luca 2008; Gotthelf et al. 2013). They have no counterparts at any other wavelength, nor associated diffuse nebulae, nor any manifestation of rotation-powered magnetospheric activity. Such sources only display steady, thermal-like X-ray emission, typically with a two-temperature blackbody spectrum and very small emitting areas. Absorption features superimposed to the continuum have been observed in two sources.

Measurement of a tiny period derivative for the only three pulsating CCOs point to very low surface dipole fields ($B_{eq} \sim 10^{11}$ G, Gotthelf et al. 2013). This is consistent with an interpretation of the absorption lines as electron cyclotron features. In this picture, it is not clear what is the origin of the apparent, relatively large thermal luminosities and large temperature anisotropies for these NSs. The spin-down luminosity is too low to explain the hot spot emission, while X-ray timing, as well as

---

[5] There are alternative hypotheses about the nature of SGR/AXPs, assuming their braking by an accretion disk (e.g., Trümper et al. 2013, and references therein) or a "magnetic slab" (Bisnovatyi-Kogan and Ikhsanov 2014), as well as the models of drift waves in the magnetosphere of a neutron star with $B \sim 10^{12}$ G (Malov 2010) or rapidly rotating massive ($M > M_{\odot}$) white dwarfs with $B \sim 10^8$ G (Boshkaev et al. 2013).

deep optical/infrared observations, rule out the existence of companion stars as well as accretion from debris discs (Halpern and Gotthelf 2010; De Luca et al. 2011). It has been suggested that a strong crustal toroidal magnetic field could channel heat from the star interior, producing hot spots on the surfaces, while not influencing the NS spin-down (see, e.g., Shabaltas and Lai 2012).

As another puzzle, the inferred, relatively high birth rate of CCOs clashes with the apparently underpopulated region of the $P - \dot{P}$ diagram in which they reside (Kaspi 2010; Halpern and Gotthelf 2010 – see Figure 1). It has been proposed that the weak observed dipole field could result from prompt accretion of $10^{-4} - 10^{-3} M_\odot$ fallback material soon after the SN explosion. The buried field would re-emerge later, on a $10^3 - 10^5$ yr time scale (depending on the amount of accreted material), turning a CCO into a RPP, or even into a magnetar (Viganò and Pons 2012).

• **The Magnificent Seven, or X-ray INSs (XINSs)**. These seven INSs were discovered in the *ROSAT All Sky Survey*. Reviews on their properties are given by Haberl (2007); Turolla (2009); Kaplan and van Kerkwijk (2009), to whom the reader is referred for more details and references.

The XINSs have spinning periods in the same range as SGR/AXPs, but the period derivative points to a dipole field $\sim 1$ order of magnitude lower for the XINSs (but still well above the one of the bulk of RPPs – see Figure 1).

These sources display a thermal-like spectrum, from the optical to the soft X-ray range.[6] Their thermal luminosity is somewhat larger than expected from conventional cooling of NSs at the same characteristic age. Broad (often multiple) spectral distortions compatible with absorption features are seen, superimposed on the thermal continuum. The nature of these features is unclear. Suggested explanations include, for example, atomic or proton-cyclotron features (e.g., Haberl 2007), photoionization in a relatively dense cloud in the vicinity of the NS (Hambaryan et al. 2009), or a result of a complex strongly inhomogeneous distribution of temperature over the surface (Viganò et al. 2014). In one case, the observed spectral shape has been tentatively explained as originated in a thin partially-ionized hydrogen atmosphere above a condensed iron surface (see Sect. 8.2).

All XINSs have an optical/UV counterpart, with a flux exceeding by a factor $5 - 50$ (around 5,000 Å) the expected value, based on the extrapolation of the soft X-ray spectrum (Kaplan et al. 2011). Such optical/UV excesses show power-law spectra, but the observed slopes differ from source to source and are generally not consistent with the Rayleigh-Jeans tail of a blackbody spectrum. The origin of the optical/UV excess is not understood (atmospheric effects? magnetospheric activity? evidence for an emitting region larger and cooler than the one seen in X-rays?).

All XINSs are steady emitters, with the exception of RX J0720.4−3125, whose time variability has not yet been understood (see Hohle et al. 2012, possible explanations range from magnetar-like activity to a peculiar accretion episode).

The XINSs are rather close (from 120 pc to a few hundred pc) to the Solar system. These distance estimates are based on direct annual parallax measurements or on

---

[6] For some of them, pulsed radio emission has been also detected at very low frequency 111 MHz at the the Pushchino Radio Astronomy Observatory – see Malofeev et al. (2007); Teplykh et al. (2011). Such detections are very intriguing and await confirmation from other observations at similar frequencies, e.g., by the LOFAR telescope.

comparison of the observed photoelectric absorption to models for the 3D distribution of local interstellar medium, and they are consistent with the large observed proper motions. Back-projection of the NS space trajectories allowed to infer a kinematic age for a few sources, based on possible association with clusters of massive stars (see e.g. Tezlaff et al. 2011). Interestingly enough, the kinematic ages are systematically smaller than characteristic ages $\tau_c$, being thus more consistent with the relatively high thermal luminosities.

It has been suggested that the magnetic field of the XINSs could have decayed since their birth, affecting their rotational and thermal evolution (Popov et al. 2010). The relationship of the XINSs to other classes of INSs is in any case still poorly understood (aged magnetars? HB RPPs with unfavorable radio beaming? extreme RRaTs?).

Unifying the apparent diversity of the classes of INSs in a coherent physical scenario is a major goal in the astrophysics of INSs. A study in this perspective was performed by Viganò et al. (2013), who modeled the coupled evolution of temperature and magnetic field (driving the rotational evolution) of INSs and proved the possibility to explain the overall properties of the classes of SGR/AXPs, HB RPPs, and of the XINSs by varying the initial magnetic field, mass and envelope composition in a unique parent population of INSs.

## 3 Isolated neutron stars with thermal spectra

Viganò et al. (2013) gathered and thoroughly re-analyzed all the best available data on isolated, thermally emitting NSs were in a consistent way. We refer the interested reader to that reference for more details. The data sample of 40 sources was compared to theoretical models of the magneto-thermal evolution of NSs, in an attempt to explain the phenomenological diversity of SGR/AXPs, high-B radio-pulsars, and isolated nearby NSs by only varying their initial magnetic field, mass and envelope composition. The cooling theory of NSs and several issues characteristic of magnetars are also discussed in other chapters of this volume. In this chapter, we focus on the thermal emission from sources not cataloged as magnetar candidates (SGR/AXPs). The sample of selected sources (see Table 1) includes:

• Eight CCOs, including the very young NS in Cassiopeia A, and the only three CCOs with measured values of $P$ and $\dot{P}$. We have ignored the other CCOs candidates, since they have spectral information with poor statistics and/or a very uncertain age of the associated SNR.
• 13 rotation powered pulsars, including the Vela pulsar and the so-called Three Musketeers (PSR B0656, PSR B1055 and the $\gamma$-ray-loud Geminga; De Luca et al. 2005). We have excluded most of the young pulsars, many of which are associated with pulsar wind nebulae, since in those cases data are compatible with non-thermal emission powered by the rotational energy loss, which is orders of magnitude larger than their X-ray luminosity (i.e. RX J0007.0+7303 in SNR CTA1; Caraveo et al. 2010). We also exclude several old pulsars (Zavlin and Pavlov 2004) with thermal emission from a tiny hot spot (a few tens of m$^2$), since the temperature of the small

| Source | $T_{bb}$ [$10^6$ K] | $R_{bb}$ [km] | $T_{nsa/rcs}$ [$10^6$ K] | $R_{nsa}$ [km] | best fit model | $T_{cool}$ [$10^6$ K] | $\log(L_{cool})$ [erg s$^{-1}$] |
|---|---|---|---|---|---|---|---|
| CXOU J185238.6+004020 | 5.1 | 0.9 | 3.37 | 3.0 | BB/nsa | < 1.1 | < 33.1 |
| 1E 1207.4−5209** | 2.2 | 9.6 | 1.7 | 7.4 | BB*/nsa* | < 0.7 | < 32.2 |
| RX J0822−4300 | 4.6 | 1.7 | 2.37 | 6.4 | BB/nsa | < 1.0 | < 32.9 |
| CXO J232327.9+584842 | 5.2 | 1.7 | 3.34 | 2.7 | BB/nsa | < 1.3 | < 33.3 |
| 1WGA J1713.4−3949 | 4.8 | 0.4 | – | – | BB+PL | – | – |
| CXOU J085201.4−461753 | 4.7 | 0.28 | 3.1 | 1.2 | BB/nsa | – | – |
| XMMU J172054.5−372652 | 4.9 | 2.6 | – | – | BB+PL | – | – |
| XMMU J173203.3−344518 | 5.7 | – | 2.6$^C$ | 13$^C$ | C atm | – | – |
| PSR J0538+2817 | 1.9 | 2.6 | – | – | BB+PL | – | < 31.9 |
| PSR B1055−52 | 2.2 | 0.3 | – | – | 2BB+PL | 0.8 | – |
| PSR J0633+1746 | 1.6 | 0.1 | – | – | 2BB+PL | 0.49 | – |
| PSR B1706−44 | 1.7 | 3.3 | – | – | BB+PL | < 0.7 | < 32.2 |
| PSR B0833−45 | 1.4 | 5.0 | 0.93 | 9.4 | (BB/nsa)+PL | < 0.5 | < 31.5 |
| PSR B0656+14 | 1.2 | 2.4 | – | – | 2BB+PL | 0.6 | – |
| PSR B2334+61 | 1.9 | 1.1 | 1.0 | 7.9 | BB/nsa | < 0.6 | < 31.9 |
| PSR J1740+1000 | 2.0 | 0.4 | 0.6 | 10.3 | 2BB/nsa | 0.9 | – |
| PSR J1741−2054 | 0.7 | 12 | – | – | BB | – | – |
| PSR J1357−6429 | 1.6 | 2.0 | 0.74 | 10.0 | (BB/nsa)+PL | – | – |
| PSR J0726−2612 | 1.0 | 4.6 | – | – | BB | < 0.46 | < 31.5 |
| PSR J1119−6127** | 3.1 | 1.5 | – | – | BB | < 1.4 | < 32.9 |
| PSR J1819−1458 | 1.5 | 12.3 | – | – | BB | – | – |
| PSR J1718−3718 | 2.2 | 2.0 | – | – | BB | < 1.0 | < 32.9 |
| RX J0420.0−5022 | 0.6 | 3.4 | – | – | BB | – | – |
| RX J1856.5−3754** | 0.73 | 4.1 | – | – | BB | – | – |
| RX J2143.0+0654 | 1.24 | 2.3 | – | – | BB | – | – |
| RX J0720.4−3125 | 0.97 | 5.7 | – | – | BB | – | – |
| RX J0806.4−4123 | 1.17 | 1.2 | 0.63 | 8.2 | BB*/nsa* | – | – |
| RX J1308.6+2127** | 1.09 | 5.0 | – | – | BB* | – | – |
| RX J1605.3+3249 | 1.15 | 0.9 | 0.49 | 7.0 | BB*/nsa* | – | – |

* Absorption line(s) gabs included in the fit.
** See discussion of a more elaborated analysis in Sect. 8.
$^C$ Fits to a carbon atmosphere and assuming $d = 3.2$ kpc.

**Table 1** Emission properties of the thermally emitting neutron stars. $T_{bb}$ and $R_{bb}$ are the temperature and radius inferred by the bbodyrad model. $T_{nsa}$ is the temperature inferred by the nsa model with acceptable associated radius $R_{nsa}$, also indicated. $T_{cool}$ is either the lower temperature for models including 2 BB, compatible with emission from the entire surface, or the upper limit for cases showing emission from a small spot $R_{bb} \sim$ a few km. In the latter case, $L_{cool}$ is the associated upper limit to the "hidden" thermal luminosity. Data are from Viganò et al. (2013) as well as from www.neutronstarcooling.info. All radii, temperatures and luminosities are the values as measured by a distant observer.

hot spots is probably unrelated to the cooling history of the NS. Our list also includes four high-B radio-pulsars magnetic fields $B_{eq} \sim 10^{13} - 10^{14}$ G and good quality spectra. We have excluded the AXP-like pulsar PSR J1846−0258 since during quiescence its X-ray emission does not show a significant thermal component (Ng et al. 2008; Livingstone et al. 2011), and it is orders of magnitude smaller than its rotational energy loss.

• We have included the only RRaT detected so far in X-ray (PSR J1819−1458).

• The Magnificent Seven (XINSs). All of them have good spectra, and most of them have well determined timing properties and good distance determinations (sometimes with direct parallax measurements).

We summarize the main properties of thermal emitters in Table 1 (taken from Viganò et al. 2013 and extended). All the data presented here with links to abundant references can also be found in the website http://www.neutronstarcooling.info/.

Although both, luminosities and temperatures can be obtained by spectral analysis, it is usually difficult to determine them accurately. The luminosity is always subject to the uncertainty in the distance measurement, while the inferred effective temperature depends on the choice of the emission model (blackbody vs. atmosphere models, composition, condensed surface, etc.), and it carries large theoretical uncertainties in the case of strong magnetic fields. We often find that more than one model can fit equally well the data, without any clear, physically motivated preference for one of them. Photoelectric absorption from interstellar medium further constitutes a source of error in temperature measurements, since the value of the hydrogen column density $N_H$ is correlated to the temperature value obtained in spectral fits. Different choices for the absorption model and the metal abundances can also yield different results for the temperature. In addition, in the very common case of the presence of inhomogeneous surface temperature distributions, only an approximation with two or three regions at different temperatures is usually employed. Moreover, in the case of data with few photons and/or strong absorption features, the temperature is poorly constrained by the fit, adding a large statistical error to the systematic one.

## 4 Atoms and matter in strong magnetic fields

A general review of the physics of matter in strong magnetic fields is given by D. Lai in this volume. Here we consider only the concepts that are crucial for the theory of formation of thermal spectra of NSs with strong magnetic fields.

### 4.1 Landau quantization

It is convenient to express the magnetic field by its strength in atomic units, $\gamma$, or in relativistic units, $b$:

$$\gamma = B/B_0 = 425.44\,B_{12}, \qquad b = \hbar\omega_c/(m_e c^2) = B/B_{QED} = B_{12}/44.14. \quad (1)$$

Here, $B_0 = m_e^2\,c\,e^3/\hbar^3$ is the atomic unit of magnetic field, $B_{12} \equiv B/10^{12}$ G, $\omega_c = eB/m_e c$ is the electron cyclotron frequency, and $B_{QED} = m_e^2 c^3/(e\hbar) = B_0/\alpha_f^2$ is the critical (Schwinger) field, above which specific effects of quantum electrodynamics (QED) become pronounced. We call a magnetic field *strong*, if $\gamma \gg 1$, and *superstrong*, if $b \gtrsim 1$.

The motion of charged particles in a magnetic field $\boldsymbol{B}$ is quantized in discrete Landau levels, whereas the longitudinal (parallel to $\boldsymbol{B}$) momentum of the particle can change continuously. In the nonrelativistic theory, the threshold excitation energy of the $N$th Landau level is $N\hbar\omega_c$ ($N = 0, 1, 2, \ldots$). In the relativistic theory, it is

$E_N = m_e c^2 (\sqrt{1 + 2bN} - 1)$. The wave functions that describe an electron in a magnetic field (Sokolov and Ternov 1986) have a characteristic transverse scale of the order of the "magnetic length" $a_m = (\hbar c / eB)^{1/2} = a_B / \sqrt{\gamma}$, where $a_B$ is the Bohr radius. The momentum projection on the magnetic field remains a good quantum number, therefore these projections have the usual Maxwellian distribution at thermodynamic equilibrium. For transverse motion, however, we have the discrete Boltzmann distribution over $N$.

In practice, Landau quantization becomes important when the electron cyclotron energy $\hbar\omega_c$ is at least comparable to both the electron Fermi energy $\varepsilon_F$ and temperature $T$ (in energy units, i.e., $10^6$ K $= 86.17$ eV). If $\hbar\omega_c$ is appreciably larger than both these energies, then most electrons reside on the ground Landau level in thermodynamic equilibrium, and the field is called *strongly quantizing*. It is the case, if conditions $\rho < \rho_B$ and $\zeta_e \gg 1$ are fulfilled simultaneously, where

$$\rho_B = \frac{m_i}{\pi^2 \sqrt{2}\, a_m^3 Z} = 7045 \frac{A}{Z} B_{12}^{3/2} \text{ g cm}^{-3}, \qquad \zeta_e = \frac{\hbar\omega_c}{T} = 134.34 \frac{B_{12}}{T_6}, \quad (2)$$

$m_i = A m_u$ is the ion mass, $m_u$ is the unified atomic mass unit, and $T_6$ is temperature in units of $10^6$ K. In NS atmospheres, these conditions are satisfied, as a rule, at $B \gtrsim 10^{11}$ G. In the opposite limit $\zeta_e \ll 1$, the field can be considered as *nonquantizing*. In the magnetospheres, which have lower densities, electrons can condensate on the lowest Landau level even at $B \sim 10^8$ G because of the violation of the LTE conditions (e.g., Mészáros 1992), but this is not the case in the photospheres (the atmospheric layers whose thermal state is determined by the radiative flux and where the observed spectrum is mainly formed; (see Potekhin 2014)).

For ions, the parameter $\zeta_e$ is replaced by

$$\zeta_i = \hbar\omega_{ci}/T = 0.0737 \, (Z/A) B_{12}/T_6. \qquad (3)$$

Here, $\omega_{ci} = ZeB/(m_i c)$ is the ion cyclotron frequency, $Ze$ is the ion charge, and $\hbar\omega_{ci} = 6.35(Z/A)B_{12}$ eV is the ion cyclotron energy. In magnetar atmospheres, where $B_{12} \gtrsim 100$ and $T_6 \lesssim 10$, the parameter $\zeta_i$ is not small, therefore the quantization of the ion motion should be taken into account. A parameter analogous to $\rho_B$ is unimportant for ions, because they are nondegenerate in NS envelopes.

## 4.2 Bound species in strong magnetic fields

As first noticed by Cohen et al. (1970), atoms with bound states should be much more abundant at $\gamma \gg 1$ than at $\gamma \lesssim 1$ in a NS atmosphere at the same temperature. This difference is caused by the magnetically-induced increase of binding energies (and decrease of size) of atoms in so-called *tightly-bound states*, which are characterized by electron-charge concentration at short distances to the nucleus. Therefore it is important to consider the bound states and bound-bound and bound-free transitions in a strong magnetic field even for light-element atmospheres, which would be almost fully ionized at $T \sim 10^5$ K in the nonmagnetic case.

Most studies of atoms in strong magnetic fields have considered an atom with an infinitely heavy (fixed in space) nucleus (see, e.g., Garstang 1977; Ruder et al. 1994,

for reviews). This model is rather crude, but it is a convenient first approximation. In this section we review this model. An outline of more accurate treatments, which take the effects of finite atomic mass into account, is given in Appendix A.

### 4.2.1 One-electron atoms and ions

The H atom in a magnetic field is well studied. At $B > 10^9$ G, its only electron resides at the ground Landau level $N = 0$. Since $N$ is fixed, the quantum state is determined by two other quantum numbers: $s = 0, 1, 2, \ldots$, which corresponds to the electron angular-momentum projection on the magnetic-field direction, $-\hbar s$, and $\nu = 0, 1, 2, \ldots$, which corresponds mainly to the motion along $\boldsymbol{B}$. The tightly-bound states all have $\nu = 0$. Their binding energies logarithmically increase with increasing $\gamma$ (asymptotically as $\sim \ln^2 \gamma$ Ry, where 1 Ry=13.6057 eV is the Rydberg constant in energy units). Non-zero values of $\nu$ correspond to loosely-bound states, whose binding energies are confined within 1 Ry.

Accurate calculations of the properties of the bound states of a non-moving H atom in a strong magnetic field have been performed in many works (see Ruder et al. 1994, for a review). The $B$-dependences of binding energies are well approximated by analytical functions (Potekhin 2014). Continuum wave functions and photoionization cross-sections have also been calculated (Potekhin et al. 1997).

In the approximation of an infinite nuclear mass, the energy of any one-electron ion is related to the H-atom energy as $E(Z_n, B) = Z_n^2 E(1, B/Z_n^2)$ (Surmelian and O'Connel 1974). Analogous similarity relations exist also for the cross sections of radiative transitions (Wunner et al. 1982). However, all these relations are violated by motion across the magnetic field. Even for an atom at rest, the account of the finite nuclear mass can be important at $s \neq 0$ (see Appendix A).

### 4.2.2 Many-electron atoms and ions

According to the Thomas-Fermi model, a typical size of an atom with a large nuclear charge $Z_n$ is proportional to $\gamma^{-2/5}$ in the interval $Z_n^{4/3} \ll \gamma \ll Z_n^3$ (Kadomtsev 1970), but this model breaks down at $\gamma \gtrsim Z_n^3$ (Lieb et al. 1992). In particular, it cannot describe the difference of the transverse and longitudinal atomic sizes, which becomes huge in such strong fields. In this case, however, a good starting approximation is the so called adiabatic approximation, which presents each electron orbital as a product of the Landau function that describes free electron motion transverse to the field (Sokolov and Ternov 1986) and a function describing a one-dimensional motion along $\boldsymbol{B}$ in an effective potential, similar to a truncated one-dimensional Coulomb potential (Haines and Roberts 1969). At $\gamma \gg Z_n^3$, all electron shells of the atom are strongly compressed in the directions transverse to the field. In the ground state, atomic sizes along and transverse to $\boldsymbol{B}$ can be estimated as (Kadomtsev and Kudryavtsev 1971)

$$l_\perp \approx \sqrt{2Z_n - 1}\, a_m, \quad l_z \approx \frac{Z_n^{-1} a_B}{\ln[\sqrt{\gamma}/(Z_n\sqrt{2Z_n - 1})]}. \tag{4}$$

In this case, the binding energy of the ground state increases with increasing $\boldsymbol{B}$ asymptotically as $E^{(0)} \sim -Z_n \hbar^2/(m_e l_z^2)$ (Kadomtsev and Kudryavtsev 1971).

Thomas-Fermi results are useful as an order-of-magnitude estimate. More accurate calculations of binding energies and oscillator strengths of many-electron atoms were performed with different methods. For atoms with small nuclear charge numbers $Z_n$, such as helium, a sufficiently accurate and practical method is the Hartree-Fock method with trial orbitals in the adiabatic approximation (Ruder et al. 1994; Miller and Neuhauser 1991; Medin et al. 2008). But the condition of applicability of the adiabatic approximation $\gamma \gg Z_n^3$ is too restrictive for larger $Z_n$. It is overcome in the mesh Hartree-Fock method, where each orbital is numerically determined as a function of the longitudinal ($z$) and radial coordinates (e.g., Ivanov and Schmelcher 2000, and references therein). This method, however, is computationally expensive. Mori and Hailey (2002) proposed a "hybrid" method, where corrections to the adiabatic Hartree approximation due to electron exchange and admixture of higher Landau levels are treated as perturbations. The latter method proved to be practical for modeling NS atmospheres containing atoms and ions of elements with $2 < Z_n \lesssim 10$, because it can provide an acceptable accuracy at moderate computational expenses.

### 4.2.3 Molecules and molecular ions

Best studied molecules and molecular ions are diatomic systems, especially the $H_2^+$ ion (Kappes and Schmelcher 1996, and references therein) and the $H_2$ molecule (Schmelcher et al. 2001, and references therein). Lai (2001) obtained approximate expressions for binding energies of low-lying levels of the $H_2$ molecule at $\gamma \gtrsim 10^3$. These energies increase approximately at the same rate $\propto (\ln \gamma)^2$ as the binding energies of tightly-bound states of the atom. In such strong fields, the ground state of the $H_2$ molecule is the state where the spins of both electrons are counter-aligned to $\boldsymbol{B}$ and the molecular axis is parallel to $\boldsymbol{B}$, unlike the weak fields where the ground state is $^1\Sigma_g$.

In moderately strong fields (with $\gamma \sim 1 - 10$), the behavior of the molecular terms is complicated. If the $H_2$ molecule is oriented along $\boldsymbol{B}$, then its states $^1\Sigma_g$ and $^3\Pi_u$ are metastable at $0.18 < \gamma < 12.3$ and decay into $^3\Sigma_u$, which is unbound (Detmer et al. 1998). It turns out, however, that the orientation along $\boldsymbol{B}$ is not optimal in this case. For example, the lowest energy is provided by the orientation of the molecule in the triplet state at $90°$ to $\boldsymbol{B}$ at $\gamma = 1$, and $37°$ at $\gamma = 10$ (Kubo 2007).

Strong magnetic fields stabilize the $He_2$ molecule and its ions $He_2^+$, $He_2^{2+}$, and $He_2^{3+}$, which do not exist in the absence of the field. Mori and Heyl (2007) have performed the most complete study of their binding energies in NS atmospheres. The ions $HeH^{++}$, $H_3^{++}$, and other exotic molecular ions, which become stable in strong magnetic fields, were also considered (see Turbiner 2007; Turbiner et al. 2010, and references therein). An evaluation of the ionization equilibrium shows that, at densities, temperatures, and magnetic fields characteristic of NSs, the abundance of such ions (as well as that of $H_2^+$ ions considered by Khersonskii 1987) is too small to affect the thermal spectrum.

There are very few results on molecules composed of atoms heavier than He. In particular, Medin and Lai (2006a) applied the density-functional method to calculations of binding energies of various molecules from $H_n$ to $Fe_n$ with $n$ from 1 through

8 at $B$ from $10^{12}$ G to $2 \times 10^{15}$ G. The earlier studies of heavy molecules in strong magnetic fields are discussed in the review by Lai (2001).

### 4.3 Atmosphere thermodynamics

According to the Bohr-van Leeuwen theorem, the magnetic field does not affect thermodynamics of classical charged particles. The situation differs in quantum mechanics. The importance of the quantum effects depends on the parameters $\zeta_e$ and $\zeta_i$ [Eqs. (2), (3)].

Studies of thermodynamics of magnetic NS atmospheres, as a rule, are based on the decomposition of the Helmholtz free energy

$$F = F_{\mathrm{id}}^{(e)} + F_{\mathrm{id}}^{(i)} + F_{\mathrm{int}} + F_{\mathrm{ex}}, \tag{5}$$

where $F_{\mathrm{id}}^{(e)}$ and $F_{\mathrm{id}}^{(i)}$ describe the ideal electron and ion gases, $F_{\mathrm{int}}$ includes internal degrees of freedom for bound states, and $F_{\mathrm{ex}}$ is a nonideal component due to interactions between plasma particles. All the necessary thermodynamic functions are then expressed through derivatives of $F$ over $\rho$ and $T$.

#### 4.3.1 Equation of state

The free energy of $N_i$ nondegenerate nonrelativistic ions is given by

$$\frac{F_{\mathrm{id}}^{(i)}}{N_i T} = \ln\left(2\pi \frac{n_i \lambda_i a_{\mathrm{m}}^2}{Z}\right) + \ln\left(1 - \mathrm{e}^{-\zeta_i}\right) - 1 + \frac{\zeta_i}{2} + \ln\left(\frac{\sinh[g_i \zeta_i (2s_i + 1)/4]}{\sinh(g_i \zeta_i/4)}\right), \tag{6}$$

where $\lambda_i = [2\pi\hbar^2/(m_i T)]^{1/2}$ is the thermal de Broglie wavelength for the ions, $s_i$ is the spin number, and $g_i$ is the spin-related g-factor (for instance, $s_i = 1/2$ and $g_i = 5.5857$ for the proton). All the terms in (6) have clear physical meanings. At $\zeta_i \to 0$, the first and second terms give together $\ln(n_i \lambda_i^3)$, which corresponds to the three-dimensional Boltzmann gas. The first term corresponds to the one-dimensional Boltzmann gas model at $\zeta_i \gg 1$. The second-last term in (6) gives the energy $\hbar\omega_{ci}/2$ of zero-point oscillations of every ion transverse to the magnetic field. Finally, the last term represents the energy of magnetic moments in a magnetic field.

The ideal electron-gas part of the free energy $F_{\mathrm{id}}^{(e)}$ can be expressed through the Fermi-Dirac integrals (see Potekhin and Chabrier 2013, for explicit expressions). In a strongly quantizing magnetic field, the electron Fermi momentum equals $p_{\mathrm{F}} = 2\pi^2 a_{\mathrm{m}}^2 \hbar n_e$, where $n_e = n_i Z$ is the electron number density. Therefore, with increasing $n_e$ at a fixed $B$, the degenerate electrons begin to fill the first Landau level when $n_e$ reaches $n_B = (\pi^2 \sqrt{2} a_{\mathrm{m}}^3)^{-1}$. This value just corresponds to the density $\rho_B$ in Eq. (2). The ratio of the Fermi momentum $p_{\mathrm{F}}$ in the strongly quantizing field to its nonmagnetic value $\hbar(3\pi^2 n_e)^{1/3}$ equals $[4\rho^2/(3\rho_B^2)]^{1/3}$. Therefore, the Fermi energy at a given density $\rho < \sqrt{3/4}\,\rho_B$ becomes smaller with increasing $B$, which means that a strongly quantizing magnetic field relieves the electron-gas degeneracy. For this reason, strongly magnetized NS atmospheres remain mostly nondegenerate, despite their

densities are orders of magnitude higher than the nonmagnetic atmosphere densities. For the nondegenerate electron gas, $F_{\mathrm{id}}^{(\mathrm{e})}$ takes the form of Eq. (6) (with the obvious replacements of $n_{\mathrm{i}}$, $\lambda_{\mathrm{i}}$, $\zeta_{\mathrm{i}}$, $g_{\mathrm{i}}$, $s_{\mathrm{i}}$, and $Z$ by $n_{\mathrm{e}}$, $\lambda_{\mathrm{e}}$, $\zeta_{\mathrm{e}}$, 2, $\frac{1}{2}$, and 1, respectively).

The nonideal free-energy part $F_{\mathrm{ex}}$ contains the Coulomb and exchange contributions of the electrons and the ions, and the electron-ion polarization energy, and also interactions of ions and electrons with atoms and molecules. In turn, the interaction between the ions is described differently depending on the phase state of matter. The terms that constitute $F_{\mathrm{ex}}$ depend on magnetic field only if it quantizes the motion of these interacting particles. Here we will not discuss these terms but address an interested reader to Potekhin and Chabrier (2013) and references therein. This non-ideality is usually negligible in the NS atmospheres, but it determines the formation of a condensed surface, which will be considered in Sect. 6.

## 4.4 Ionization equilibrium

For atmosphere simulations, it is necessary to determine the fractions of different bound states, because they affect the spectral features that are caused by bound-bound and bound-free transitions. The solution to this problem is laborious and ambiguous. The principal difficulty in the chemical model of plasmas, namely the necessity to distinguish the bound and free electrons and "attribute" the bound electrons to certain nuclei, becomes especially acute at high densities, where the atomic sizes cannot be anymore neglected with respect to their distances. Current approaches to the solution of this problem are based, as a rule, on the concept of the so-called occupation probabilities of quantum states.

Let us consider a quantum state $\kappa$ of an ion lacking $j$ electrons, with binding energy $E_{j,\kappa}$ and quantum statistical weight $g_{j,\kappa}$. An occupation probability $w_{j,\kappa}$ is an additional statistical weight of this quantum state, caused by interactions with surrounding plasma (in general, this weight is not necessarily less than unity, therefore it is not quite a probability). As first noted by Fermi (1924), occupation probabilities $w_{j,\kappa}$ cannot be arbitrary but should be consistent with $F_{\mathrm{ex}}$. Minimizing $F$ with account of the Landau quantization leads to a system of ionization-equilibrium equations for $n_j \equiv \sum_\kappa n_{j,\kappa}$ (e.g., Rajagopal et al. 1997)

$$\frac{n_j}{n_{j+1}} = \frac{n_{\mathrm{e}} \lambda_{\mathrm{e}}^3}{2} \frac{\sinh \zeta_j}{\zeta_j} \frac{\zeta_{j+1}}{\sinh \zeta_{j+1}} \frac{\tanh \zeta_{\mathrm{e}}}{\zeta_{\mathrm{e}}} \frac{\mathscr{Z}_{\mathrm{int},j}}{\mathscr{Z}_{\mathrm{int},j+1}} \exp\left(\frac{E_{j,\mathrm{ion}}}{T}\right), \tag{7}$$

where $\mathscr{Z}_{\mathrm{int},j} = \sum_\kappa g_{j,\kappa} w_{j,\kappa} \exp\left[(E_{j,\kappa} - E_{j,\mathrm{gr.st}})/(T)\right]$ is internal partition function for the $j$th ion type, $E_{j,\mathrm{gr.st}}$ is its ground-state binding energy, $E_{j,\mathrm{ion}} = E_{j,\mathrm{gr.st}} - E_{j+1,\mathrm{gr.st}}$ is its ionization energy, and $\zeta_j$ is the magnetic quantization parameter (3). Equation (7) differs from the usual Saha equation, first, by the terms with $\zeta_{\mathrm{e}}$ and $\zeta_j$, representing partition functions for distributions of free electrons and ions over the Landau levels, and second, by the occupation probabilities $w_{j,\kappa}$ in the expressions for the partition functions $\mathscr{Z}_{\mathrm{int},j}$. Here, $w_{j,\kappa}$ are the thermodynamic occupation probabilities, which determine the complete destruction of an atom with increasing pressure.

They should not be confused with the optical occupation probabilities, which determine dissolution of spectral lines because of the Stark shifts in plasma microfields (see Potekhin 1996 for discussion and references).

Equation Eq. (7) was applied to modeling partially ionized atmospheres of NSs, composed of iron, oxygen, and neon (Rajagopal et al. 1997; Mori and Hailey 2006; Mori and Ho 2007). The effects related to the finite nuclear masses (Appendix A) were either ignored or treated as a small perturbation. A more accurate treatment, which rigorously takes these effects into account, is outlined in Appendix A.2.

## 5 Formation of spectra in strongly magnetized atmospheres

### 5.1 Radiative transfer in normal modes

Propagation of electromagnetic waves in magnetized plasmas was studied in many works, the book by Ginzburg (1970) being the most complete of them. At radiation frequency $\omega$ much larger than the electron plasma frequency $\omega_{pe} = \left(4\pi e^2 n_e / m_e^*\right)^{1/2}$, where $m_e^* \equiv m_e \sqrt{1 + p_F^2/(m_e c)^2}$, the waves propagate in the form of two polarization modes, extraordinary (hereafter denoted by subscript $j = 1$) and ordinary ($j = 2$). They have different polarization vectors $e_j$ and different absorption and scattering coefficients, which depend on the angle $\theta_B$ between $B$ and the wave vector $k$. The modes interact with each another through scattering. Gnedin and Pavlov (1974) formulated the radiative transfer problem in terms of these modes. They showed that in strongly magnetized NS atmospheres a strong Faraday depolarization occurs, except for narrow frequency ranges near resonances. Therefore, it is sufficient to consider specific intensities of the two normal modes instead of the four components of the Stokes vector. The radiative transfer equation for these specific intensities is (Kaminker et al. 1982)

$$\cos\theta_k \frac{\mathrm{d}I_{\omega,j}(\hat{\mathbf{k}})}{\mathrm{d}y_{col}} = \varkappa_{\omega,j}(\hat{\mathbf{k}})I_{\omega,j}(\hat{\mathbf{k}}) - \varkappa_{\omega,j}^a(\hat{\mathbf{k}})\frac{\mathscr{B}_{\omega,T}}{2} - \sum_{j'=1}^{2}\int_{(4\pi)}\varkappa_{\omega,j'j}^s(\hat{\mathbf{k}}',\hat{\mathbf{k}})I_{\omega,j'}(\hat{\mathbf{k}}')\,\mathrm{d}\hat{\mathbf{k}}',$$
(8)

where $\hat{\mathbf{k}} = \mathbf{k}/|k|$ is the unit vector along the wave vector $\mathbf{k}$, $y_{col} = \int_r^\infty (1+z_g)\rho(r)\mathrm{d}r$ is the column density, and the factor $(1+z_g)$ is the relativistic scale change in the gravitational field, $z_g$ being the surface redshift (see Sect. 7). Here, $I_{\omega,j}$ denotes the specific intensity of the polarization mode $j$ per unit circular frequency (if $I_\nu$ is the specific intensity per unit frequency, then $I_\omega = I_\nu/(2\pi)$; see Zheleznyakov 1996), $\mathscr{B}_{\omega,T} = (\hbar\omega^3/4\pi^3 c^2)(e^{\hbar\omega/T} - 1)^{-1}$ is the specific intensity of nonpolarized blackbody radiation, and

$$\varkappa_{\omega,j}(\hat{\mathbf{k}}) \equiv \varkappa_{\omega,j}^a(\hat{\mathbf{k}}) + \sum_{j'=1}^{2}\int_{(4\pi)}\varkappa_{\omega,j'j}^s(\hat{\mathbf{k}}',\hat{\mathbf{k}})\,\mathrm{d}\hat{\mathbf{k}}',$$
(9)

The dependence of the absorption and scattering opacities $\varkappa^a, \varkappa^s$ on ray directions $(\hat{\mathbf{k}}, \hat{\mathbf{k}}')$ is affected by $B$. Therefore, the emission of a magnetized atmosphere, unlike

the nonmagnetic case, depends not only on the angle $\theta_k$ between the ray and the normal direction to the stellar surface, $\theta_n$, but also on the angle $\theta_n$ between $\boldsymbol{B}$ and the normal, and the angle $\varphi_k$ between the projections of $\boldsymbol{B}$ and $\boldsymbol{k}$ onto the surface.

In the plane-parallel limit, and assuming that the magnetic field is constant in the thin photospheric layer, the equations for hydrostatic and energy balance are the same as in the absence of magnetic field (see, e.g., Suleimanov et al. 2012b):

$$\frac{dP}{dy_{\rm col}} = g - g_{\rm rad}, \qquad g_{\rm rad} \approx \frac{2\pi}{c} \int_0^\infty d\omega\, \varkappa_\omega \int_0^\pi \cos\theta_k\, I_\omega(\hat{\mathbf{k}}) \sin\theta_k\, d\theta_k. \tag{10}$$

$$\int_0^\infty d\omega \int_{(4\pi)} I_\omega(\hat{\mathbf{k}}) \cos\theta_k\, d\hat{\mathbf{k}} = F_{\rm ph}, \tag{11}$$

where $I_\omega = \sum_{j=1}^2 I_{\omega,j}$ is the total specific intensity.

The diffusion equation for the normal modes was derived by Kaminker et al. (1982). For the plane-parallel atmosphere it reads (Zavlin 2009)

$$\frac{d}{dy_{\rm col}} D_{\omega,j} \frac{d}{dy_{\rm col}} J_{\omega,j} = \bar{\varkappa}_{\omega,j}^{\rm a} \left[ J_{\omega,j} - \frac{\mathscr{B}_{\omega,T}}{2} \right] + \bar{\varkappa}_{\omega,12}^{\rm s} \left[ J_{\omega,j} - J_{\omega,3-j} \right]. \tag{12}$$

Here,

$$\bar{\varkappa}_{\omega,j}^{\rm a} = \frac{1}{4\pi} \int_{(4\pi)} \varkappa_{\omega,12}^{\rm a}\, d\hat{\mathbf{k}}, \qquad \bar{\varkappa}_{\omega,j}^{\rm s} = \frac{1}{4\pi} \int_{(4\pi)} d\hat{\mathbf{k}}' \int_{(4\pi)} d\hat{\mathbf{k}}\, \varkappa_{\omega,12}^{\rm s}(\hat{\mathbf{k}}',\hat{\mathbf{k}}), \tag{13}$$

$$J_{\omega,j} = \frac{1}{4\pi} \int_{(4\pi)} I_{\omega,j}(\hat{\mathbf{k}})\, d\hat{\mathbf{k}}, \qquad D_{\omega,j} = \frac{1}{3\varkappa_{\omega,j}^{\rm eff}} = \frac{\cos^2\theta_n}{3\varkappa_{\omega,j}^{\|}} + \frac{\sin^2\theta_n}{3\varkappa_{\omega,j}^{\perp}}, \tag{14}$$

$$\left\{ \begin{array}{l} (\varkappa_j^{\|})^{-1} \\ (\varkappa_j^{\perp})^{-1} \end{array} \right\} = \frac{3}{4} \int_0^\pi \left\{ \begin{array}{l} 2\cos^2\theta_B \\ \sin^2\theta_B \end{array} \right\} \frac{\sin\theta_B\, d\theta_B}{\varkappa_j(\theta_B)}. \tag{15}$$

The effective opacity for nonpolarized radiation is $\varkappa^{\rm eff} = 2/(3D_{\omega,1} + 3D_{\omega,2})$. The diffusion approximation (12) serves as a starting point in an iterative method (Shibanov and Zavlin 1995), which allows one to solve the system (8) more accurately.

## 5.2 Plasma polarizability

In Cartesian coordinates with the $z$-axis along $\boldsymbol{B}$, the plasma dielectric tensor is (Ginzburg 1970)

$$\boldsymbol{\varepsilon} = \mathbf{I} + 4\pi\boldsymbol{\chi} = \begin{pmatrix} \varepsilon_\perp & i\varepsilon_\wedge & 0 \\ -i\varepsilon_\wedge & \varepsilon_\perp & 0 \\ 0 & 0 & \varepsilon_\| \end{pmatrix}, \tag{16}$$

where $\mathbf{I}$ is the unit tensor, $\boldsymbol{\chi} = \boldsymbol{\chi}^{\rm H} + i\boldsymbol{\chi}^{\rm A}$ is the complex polarizability tensor of plasma, $\boldsymbol{\chi}^{\rm H}$ and $\boldsymbol{\chi}^{\rm A}$ are its Hermitian and anti-Hermitian parts, respectively. This tensor becomes diagonal in the cyclic (or rotating) coordinates with unit vectors $\hat{\mathbf{e}}_{\pm 1} = (\hat{\mathbf{e}}_x \pm i\hat{\mathbf{e}}_y)/\sqrt{2}$, $\hat{\mathbf{e}}_0 = \hat{\mathbf{e}}_z$. Under the assumption that the electrons and ions lose

their regular velocity, acquired in an electromagnetic wave, by collisions with an effective frequency $\nu_{\rm eff}$ independent of the velocities, then the cyclic components of the polarizability tensor are (Ginzburg 1970, Sect. 10)

$$\chi_\alpha = -\frac{1}{4\pi}\frac{\omega_{\rm pe}^2}{(\omega + \alpha\omega_{\rm c})(\omega - \alpha\omega_{\rm ci}) + {\rm i}\omega\nu_{\rm eff}} \qquad (17)$$

($\alpha = 0, \pm 1$). A more rigorous kinetic theory leads to results which cannot be described by Eq. (17) with the same frequency $\nu_{\rm eff}$ for the Hermitian and anti-Hermitian components $\chi_\alpha^{\rm H}$ and $\chi_\alpha^{\rm A}$ (Ginzburg 1970, Sect. 6).

The anti-Hermitian part of the polarizability tensor determines the opacities: $\varkappa_\alpha(\omega) = 4\pi\omega\chi_\alpha^{\rm A}(\omega)/(\rho c)$. Then the Kramers-Kronig relation gives (Bulik and Pavlov 1996; Potekhin et al. 2004)

$$\chi_\alpha^{\rm H}(\omega) = \frac{c\rho}{4\pi^2\omega}\left\{\int_0^\omega\left[\varkappa_\alpha(\omega+\omega') - \varkappa_\alpha(\omega-\omega')\right]\frac{{\rm d}\omega'}{\omega'}\right.$$
$$\left. + \int_{2\omega}^\infty\frac{\varkappa_\alpha(\omega')}{\omega'-\omega}\,{\rm d}\omega' - \int_0^\infty\frac{\varkappa_{-\alpha}(\omega')}{\omega'+\omega}\,{\rm d}\omega'\right\}. \qquad (18)$$

Thus we can calculate the polarizability tensor $\boldsymbol{\chi}$ from the opacities $\varkappa_\alpha(\omega)$.

## 5.3 Vacuum polarization

In certain ranges of density $\rho$ and frequency $\omega$, normal-mode properties are dramatically affected by a specific QED effect called vacuum polarization. The influence of the vacuum polarization on the NS emission was studied in detail by Pavlov and Gnedin (1984). If the vacuum polarization is weak, then it can be linearly added to the plasma polarization. Then the complex dielectric tensor can be written as $\boldsymbol{\varepsilon}' = \mathbf{I} + 4\pi\boldsymbol{\chi} + 4\pi\boldsymbol{\chi}^{\rm vac}$, where $\boldsymbol{\chi}^{\rm vac} = (4\pi)^{-1}\,{\rm diag}(\bar{a}, \bar{a}, \bar{a}+\bar{q})$ is the vacuum polarizability tensor, and ${\rm diag}(\dots)$ denotes the diagonal matrix. The magnetic susceptibility of vacuum is determined by expression $\boldsymbol{\mu}^{-1} = \mathbf{I} + {\rm diag}(\bar{a}, \bar{a}, \bar{a}+\bar{m})$. Adler (1971) obtained the vacuum polarizability coefficients $\bar{a}$, $\bar{q}$, and $\bar{m}$ that enter these equations in an explicit form at $b \ll 1$, Heyl and Hernquist (1997) expressed them in terms of special functions in the limits of $b \ll 1$ and $b \gg 1$. Kohri and Yamada (2002) presented their numerical calculations. Finally, Potekhin et al. (2004) described them by simple analytic expressions.

$$\bar{a} = -\frac{2\alpha_{\rm f}}{9\pi}\ln\left(1 + \frac{b^2}{5}\frac{1 + 0.25487\,b^{3/4}}{1 + 0.75\,b^{5/4}}\right), \quad \bar{q} = \frac{7\alpha_{\rm f}}{45\pi}b^2\frac{1 + 1.2\,b}{1 + 1.33\,b + 0.56\,b^2},$$
$$\bar{m} = -\frac{\alpha_{\rm f}}{3\pi}\frac{b^2}{3.75 + 2.7\,b^{5/4} + b^2}. \qquad (19)$$

The coefficients $\bar{a}$, $\bar{q}$, and $\bar{m}$ are not small at $B \gtrsim 10^{16}$ G. In this case, the vacuum refraction coefficients substantially differ from unity, and the vacuum that surrounds a NS acts as a birefringent lens, which distorts and additionally polarizes thermal radiation (Heyl and Shaviv 2002; van Adelsberg and Perna 2009). At weaker $B$, the vacuum polarization results in a resonance, which manifests in a mutual conversion of normal modes, which will be considered in Sect. 5.6.

## 5.4 Polarization vectors of the normal modes

Shafranov (1967) obtained the polarization vectors $\boldsymbol{e}_j$ for fully ionized plasmas. Ho and Lai (2003) presented their convenient expressions in terms of the coefficients $\varepsilon_\perp$, $\varepsilon_\parallel$, $\varepsilon_\wedge$, $\bar{a}$, $\bar{q}$, and $\bar{m}$, including the contributions of electrons, ions, and vacuum polarization. In the Cartesian coordinate system ($xyz$) with the $z$-axis along the wave vector $\boldsymbol{k}$ and with $\boldsymbol{B}$ in the plane $x$–$z$, one has

$$\boldsymbol{e}_j = \begin{pmatrix} e_{j,x} \\ e_{j,y} \\ e_{j,z} \end{pmatrix} = \frac{1}{\sqrt{1 + K_j^2 + K_{z,j}^2}} \begin{pmatrix} iK_j \\ 1 \\ iK_{z,j} \end{pmatrix}, \tag{20}$$

where

$$K_j = \beta \left\{ 1 + (-1)^j \left[ 1 + \frac{1}{\beta^2} + \frac{\bar{m}}{1+\bar{a}} \frac{\sin^2 \theta_B}{\beta^2} \right]^{1/2} \right\}, \tag{21}$$

$$K_{z,j} = -\frac{(\varepsilon_\perp' - \varepsilon_\parallel')K_j \cos \theta_B + \varepsilon_\wedge}{\varepsilon_\perp' \sin^2 \theta_B + \varepsilon_\parallel' \cos^2 \theta_B} \sin \theta_B, \tag{22}$$

$$\beta = \frac{\varepsilon_\parallel' - \varepsilon_\perp' + \varepsilon_\wedge^2/\varepsilon_\perp' + \varepsilon_\parallel' \bar{m}/(1+\bar{a})}{2\,\varepsilon_\wedge} \frac{\varepsilon_\perp'}{\varepsilon_\parallel'} \frac{\sin^2 \theta_B}{\cos \theta_B}, \tag{23}$$

$\varepsilon_\perp' = \varepsilon_\perp + \bar{a}$, and $\varepsilon_\parallel' = \varepsilon_\parallel + \bar{a} + \bar{q}$.

## 5.5 Opacities

In the approximation of isotropic scattering, at a given frequency $\omega$, the opacities can be presented in the form (e.g., Kaminker et al. 1982)

$$\varkappa_j^{\mathrm{a}} = \sum_{\alpha=-1}^{1} |e_{j,\alpha}(\theta_B)|^2 \frac{\sigma_\alpha^{\mathrm{a}}}{m_{\mathrm{i}}}, \quad \varkappa_{jj'}^{\mathrm{s}} = \frac{3}{4} \sum_{\alpha=-1}^{1} |e_{j,\alpha}(\theta_B)|^2 \frac{\sigma_\alpha^{\mathrm{s}}}{m_{\mathrm{i}}} \int_0^\pi |e_{j',\alpha}(\theta_B')|^2 \sin \theta_B' \, \mathrm{d}\theta_B', \tag{24}$$

where $\sigma_\alpha^{\mathrm{a,s}}$ are the absorption and scattering cross sections for the three basic polarizations. These include contributions of photon interaction with free electrons or ions (free-free transitions) as well as with bound states of atoms and ions (bound-bound and bound-free transitions).

Figure 2 shows basic opacities ($\sigma_\alpha^{\mathrm{a}}/m_{\mathrm{i}}$ in Eq. (24)) at $B = 3 \times 10^{13}$ G, $\rho = 1$ g cm$^{-3}$ and $T = 3.16 \times 10^5$ K (the left panel) and corresponding normal-mode absorption opacities $\varkappa_j^{\mathrm{a}}$ for $\theta_B = 10°$. One can clearly distinguish the features reflecting the peaks at the ion cyclotron frequency and the resonant atomic frequencies, and the line crossings related to the behavior of the plasma polarizability as function of frequency. For comparison, we show also opacities for the fully ionized plasma model under the same conditions. They miss the features related to the atomic resonances, and their values is underestimated by orders of magnitude in a wide frequency range. In the remaining of this subsection we extend our discussion about the form of the different contributions to the opacity.
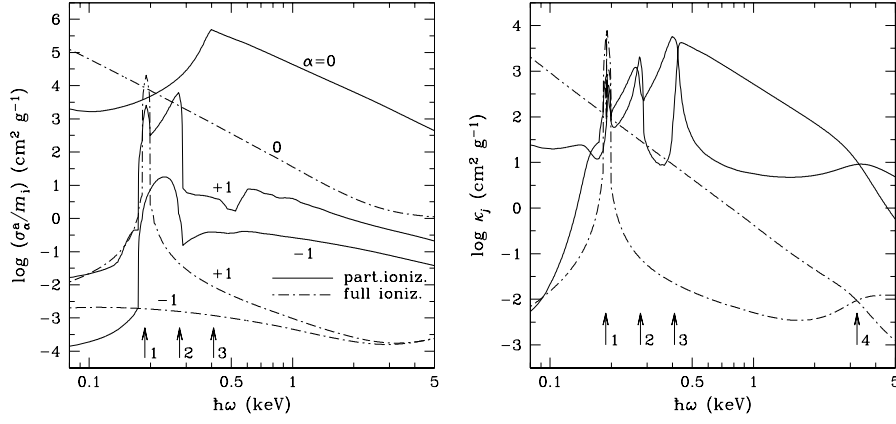
**Fig. 2** Logarithm of spectral opacities of a H plasma at $B = 3 \times 10^{13}$ G, $T = 3.16 \times 10^5$ K, $\rho = 1$ g cm$^{-3}$. Solid curves: partially ionized plasma model; dot-dashed curves: fully-ionized plasma model. *Left panel*: basic opacities for $\alpha = 0, \pm 1$. *Right panel*: opacities for two normal modes $j = 1, 2$ propagating at the angle $\theta_B = 10°$ to the field lines; the lower (upper) curve of each type corresponds to the extraordinary (ordinary) wave. The arrows indicate the features at resonant frequencies: 1– the ion cyclotron resonance $\omega = \omega_{ci}$; 2 – energy threshold for a transition between the lowest two levels $\hbar\omega = |E_{0,0}^{(0)} - E_{1,0}^{(0)}|$; 3 – the ground-state binding energy $\hbar\omega = |E_{0,0}^{(0)}|$; 4 (at the right panel) – the vacuum resonance.

### 5.5.1 Scattering

Scattering cross-sections in NS atmospheres are well known (Ventura 1979; Kaminker et al. 1982; Mészáros 1992). For $\alpha = -1$, the photon-electron scattering has a resonance at $\omega_c$. Outside a narrow (about the Doppler width) frequency interval around $\omega_c$, the cross sections for the basic polarizations $\alpha = 0, \pm 1$ are

$$\sigma_\alpha^{s,e} = \frac{\omega^2}{(\omega + \alpha\omega_c)^2 + v_{e,\alpha}^2} \sigma_T, \tag{25}$$

where $\sigma_T = (8\pi/3)(e^2/m_e c^2)^2$ is the nonmagnetic Thomson cross section, and $v_{e,\alpha}$ are effective damping factors (see below).

The photon-ion scattering cross section looks analogously,

$$\sigma_\alpha^{s,i} = \left(\frac{m_e}{m_i}\right)^2 \frac{\omega^2 Z^4}{(\omega - \alpha\omega_{ci})^2 + v_{i,\alpha}^2} \sigma_T. \tag{26}$$

Unlike the nonmagnetic case, in superstrong fields one cannot neglect the scattering on ions, because of the resonance at $\omega_{ci}$. In each case, the damping factor $v_{e,\alpha}$ or $v_{i,\alpha}$ is equal to half of the total rate of spontaneous and collisional decay of the state with energy $\hbar\omega$ (see discussion in Potekhin and Lai 2007). The spontaneous decay rates are

$$2v_e^s = \frac{4}{3} \frac{e^2}{m_e c^3} \omega^2, \quad 2v_i^s = \frac{4}{3} \frac{(Ze)^2}{m_i c^3} \omega^2. \tag{27}$$

As shown by Potekhin and Chabrier (2003) for a proton-electron plasma, the damping factors including the scattering and free-free processes can be approximately written as

$$\nu_{e,\alpha} = \nu_e^s + \nu_\alpha^{ff}(\omega_c), \quad \nu_{e,\alpha} = \nu_e^s + (m_e/m_i)\nu_\alpha^{ff}(\omega_{ci}), \tag{28}$$

where $\nu_\alpha^{ff}(\omega)$ is the effective free-free frequency given by Eq. (31) below.

*5.5.2 Absorption*

Without magnetic field, absorption or emission of a photon by a free electron is impossible without involvement of another particle, which would accept the difference between the values of the total momentum of the electron and the photon before and after the absorption. In a quantizing magnetic field, a photon can be absorbed or emitted by a free electron in a transition between Landau levels. In the nonrelativistic or dipole approximation, such transitions occur between the neighboring levels at the frequency $\omega_c$. In the relativistic theory, the multipole expansion leads to an appearance of cyclotron harmonics (Zheleznyakov 1996). Absorption cross-sections at these harmonics were derived by Pavlov et al. (1980) in the Born approximation without allowance for the magnetic quantization of electron motion, and represented in a compact form by Suleimanov et al. (2012a).

The quantization of electron motion leads to the appearance of cyclotron harmonics in the nonrelativistic theory as well. Pavlov and Panov (1976) derived photon absorption cross-sections for an electron which moves in a magnetic field and interacts with a nonmoving point charge. This model is applicable at $\omega \gg \omega_{ci}$. In the superstrong field of magnetars, the latter condition is unacceptable. A more accurate treatment of absorption of a photon by the system of a finite-mass ion and an electron yields (Potekhin and Chabrier 2003; Potekhin 2010)

$$\sigma_\alpha^{ff}(\omega) = \frac{4\pi e^2}{m_e c} \frac{\omega^2 \nu_\alpha^{ff}(\omega)}{(\omega + \alpha\omega_c)^2(\omega - \alpha\omega_{ci})^2 + \omega^2 \tilde{\nu}_\alpha^2(\omega)}, \tag{29}$$

where $\nu_\alpha^{ff}$ is an effective photoabsorption collision frequency, and $\tilde{\nu}_\alpha$ is a damping factor. In the electron-proton plasma, taking into account the scattering and free-free absorption, we have (Potekhin and Chabrier 2003)

$$\tilde{\nu}_\alpha = (1 + \alpha\omega_c/\omega)\nu_{i,\alpha}(\omega) + (1 - \alpha\omega_{ci}/\omega)\nu_{e,\alpha}(\omega) + \nu_\alpha^{ff}(\omega). \tag{30}$$

We see from (29) that $\sigma_{-1}^{ff}$ and $\sigma_{+1}^{ff}$ have a resonance at the frequencies $\omega_c$ and $\omega_{ci}$, respectively. The effective free-free absorption frequency can be written as

$$\nu_\alpha^{ff}(\omega) = \frac{4}{3}\sqrt{\frac{2\pi}{m_e T}} \frac{n_e e^4}{\hbar\omega} \Lambda_\alpha^{ff}(\omega), \tag{31}$$

where $\Lambda_\alpha^{ff}(\omega)$ is a dimensionless Coulomb logarithm ($\Lambda_\alpha^{ff} = (\pi/\sqrt{3})g_\alpha^{ff}$, where $g_\alpha^{ff}$ is a Gaunt factor). Without the magnetic field, $\Lambda_\alpha^{ff}$ is a smooth function of $\omega$. In a quantizing magnetic field, however, it has peaks at the multiples of both the electron and ion cyclotron frequencies for all polarizations $\alpha$. However, these two types of peaks are different. Unlike the electron cyclotron harmonics, the ion cyclotron harmonics are so weak that they can be safely neglected in the NS atmospheres (see Potekhin 2010).

*5.5.3 Bound-bound and bound-free transitions.*

The calculation of the cross section of photons with bound states of atoms and ions is very complex. It implies averaging of the cross sections of photon and atom absorption over all values of $K_\perp$. Since the distribution over $K_\perp$ is continuous for the atoms and discrete for the ions, such averaging for atoms reduces to an integration over $K_\perp$, analogous to Eq. (45), whereas for ions it implies summation with an appropriate statistical weight. To date, such calculation has been realized for atoms of hydrogen (Potekhin and Chabrier 2003, 2004) and helium (Mori and Heyl 2007). In the Appendix, we briefly discuss different issues related to bound states and their interaction with photons with the account of atomic thermal motion in strong magnetic fields.

## 5.6 Spectra of magnetic atmospheres

Shibanov et al. (1992) calculated spectra from strongly magnetized NS atmospheres, which was assumed to be fully ionized. Later they created a database of model spectra (Pavlov et al. 1995) and included it in the *XSPEC* package (Arnaud 1996) under the name NSA. They have shown that the spectra of magnetic hydrogen and helium atmospheres are softer than the respective nonmagnetic spectra, but harder than the blackbody spectrum with the same temperature. In addition to the spectral energy distribution, these authors have also studied the polar diagram and polarization of the outgoing emission, which proved to be quite nontrivial because of redistribution of energy between the normal modes. The thermal radiation of a magnetized atmosphere is strongly polarized, and the polarization sharply changes at the cyclotron resonance with increasing frequency. At contrast to the isotropic blackbody radiation, radiation of a magnetic atmosphere consists of a narrow ($< 5°$) pencil beam along the magnetic field and a broad fan beam with typical angles $\sim 20° - 60°$ (Zavlin et al. 1995; see also van Adelsberg and Lai 2006). These calculations have thus fully confirmed the early analysis by Gnedin and Sunyaev (1974). Later, analogous calculations were performed by other research groups (Zane et al. 2001; Ho and Lai 2003; van Adelsberg and Lai 2006). They paid special attention to manifestations of the ion cyclotron resonance in observed spectra, which was suggested by some SGR/AXP data. Lai and Ho (2002) showed that vacuum polarization leads to a conversion of the normal modes: a photon related to one mode transforms, with certain probability, into a photon of the other mode while crossing a surface with a certain critical density, depending of the photon energy as

$$\rho = 0.00964 \,(A/Z)\,(\hbar\omega/\text{keV})^2\,B_{12}^2/f_B^2 \text{ g cm}^{-3}, \tag{32}$$

where $f_B^2 = \alpha_f b^2/[15\pi(\bar{q}+\bar{m})]$, while $\bar{q}$ and $\bar{m}$ are the vacuum-polarization coefficients (Sect. 5.3); $f_B \approx 1$ at $B \lesssim 10^{14}$ G. The energy $\hbar\omega$ in Eq. (32) corresponds to the line crossing in Fig. 2, indicated by arrow labelled '4'. It follows from Eq. (32) that for $B \sim 10^{14}$ G this energy coincides with the ion cyclotron energy at the density where the atmosphere is optically thin for the extraordinary mode, but optically

thick for the ordinary mode. Under such conditions, the mode conversion strongly suppresses the ion cyclotron feature in the emission spectrum.

For the first computations of partially ionized atmospheres of NSs with magnetic fields $B \sim 10^{12} - 10^{13}$ G (Miller 1992; Rajagopal et al. 1997), the properties of atoms in magnetic fields were calculated by the adiabatic Hartree-Fock method (Miller and Neuhauser 1991). The atomic motion was either ignored (Miller 1992) or treated approximately by the perturbation theory (Rajagopal et al. 1997). Later, Potekhin et al. (2004) constructed a strongly magnetized hydrogen atmosphere model beyond the framework of the adiabatic approximation, including partial ionization and effects of the atomic motion. The calculated spectra revealed a narrow absorption line at the proton cyclotron energy and some features related to atomic transitions. As well as in the fully ionized plasma model, the intensity has a maximum at higher energies relative to the maximum of the Planck function, but at lower energies relative to the nonmagnetic H atmosphere model. Therefore, the model of a fully-ionized atmosphere with a strong magnetic field can yield a realistic temperature, but does not reproduce the spectral features caused by atomic transitions.

## 6 A condensed surface as an alternative to gaseous atmospheres

Ruderman (1971) suggested that a strong magnetic field can stabilize polymer chains directed along the field lines, and that the dipole-dipole attraction of these chains may result in a condensed phase. Later works confirmed this conjecture, but the binding and sublimation energies turned out to be smaller than Ruderman assumed (see Medin and Lai 2006b, and references therein).

From the thermodynamics point of view, the magnetic condensation is nothing but the plasma phase transition caused by the strong electrostatic attraction between the ionized plasma particles. This attraction gives a negative contribution to pressure $P_{ex}$, which, at low temperatures, is not counterbalanced until the electrons become degenerate with increasing density. In the absence of a magnetic field, such phase transitions were studied theoretically since 1930s (see Ebeling and Norman 2003, for a review). In this case, the temperature of the outer layers of a NS $T \gtrsim (10^5 - 10^6)$ K exceeds the critical temperature $T_{crit}$ for the plasma phase transition. However, we have seen in Sect. 4.3.1 that a quantizing magnetic field lifts electron degeneracy. As a result, $T_{crit}$ increases with increasing $B$, which may enable such phase transition.

Lai (2001) estimated the condensed-surface density as

$$\rho_s \approx 561 \, \eta \, A Z^{-3/5} B_{12}^{6/5} \text{ g cm}^{-3}, \tag{33}$$

where $\eta$ is an unknown factor of the order of unity. In the ion-sphere model (Salpeter 1961), the electrons are replaced by a uniform negative background, and the potential energy per ion is estimated as the electrostatic energy of the ionic interaction with the negative background contained in the sphere of radius $a_i = (4\pi n_i/3)^{-1/3}$. By equating $|P_{ex}|$ to the pressure of degenerate electrons, one obtains Eq. (33) with $\eta = 1$. This estimate disregards the effects of ion correlations, electron-gas polarizability, and bound state formation. Applying different versions of the Thomas-Fermi method

to the treatment of the electron polarization, one gets quite different results: for example, the zero-temperature Thomas-Fermi results for Fe at $10^{10}$ G $\leqslant B \leqslant 10^{13}$ G (Rögnvaldsson et al. 1993) can be described by Eq. (33) with $\eta \approx 0.2 + 0.01/B_{12}^{0.56}$, and in a finite-temperature Thomas-Fermi model (Thorolfsson et al. 1998) there is no phase transition at all.

Medin and Lai (2006b, 2007) estimated the condensation energy by the density functional method and calculated the equilibrium density of a saturated vapor of the atoms and polymer chains of helium, carbon, and iron above the respective condensed surfaces at $1 \lesssim B_{12} \leqslant 10^3$. By equating this density to $\rho_s$, they found $T_{crit}$ at several $B$ values. Unlike previous authors, Medin and Lai (2006b, 2007) have considered the electron band structure in the condensed phase. Their results for $\rho_s$ can be described by Eq. (33) with $\eta = 0.517 + 0.24/B_{12}^{1/5} \pm 0.011$ for carbon and $\eta = 0.55 \pm 0.11$ for iron, and the critical temperature can be evaluated as $T_{crit} \sim 5 \times 10^4 Z^{1/4} B_{12}^{3/4}$ K (Potekhin and Chabrier 2013).

When magnetic field increases from $10^{12}$ G to $10^{15}$ G, the cohesive energy, calculated by Medin and Lai (2007) for the condensed surface, varies monotonically from 0.07 keV to 5 keV for helium, from 0.05 keV to 20 keV for carbon, and from 0.6 keV to 70 keV for iron. The power-law interpolation between these limits roughly agrees with numerical results. The electron work function changes in the same $B$ range from 100 eV to $(600 \pm 50)$ eV. With the calculated energy values, Medin and Lai (2007) determined the conditions of electron and ion emission in the vacuum gap above the polar cap of a pulsar and the conditions of gap formation, and calculated the pulsar "death lines".

### 6.1 Radiation from a naked neutron star

For NSs with a liquid or solid condensed surface, the formation of thermal spectra depends on its reflectivity, first calculated by Itoh (1975) and Lenzen and Trümper (1978) under simplifying assumptions. Detailed calculations of the reflection properties of a strongly magnetized metallic surface were presented by Brinkmann (1980) and revisited in several more recent papers (Turolla et al. 2004; van Adelsberg et al. 2005; Pérez-Azorín et al. 2005; Potekhin et al. 2012). The authors determined the normal-mode polarization vectors in the medium under the surface, expressed the complex refraction coefficients as functions of the angles $\theta_k$ and $\varphi_k$ that determine the direction of a reflected ray, and expanded the complex electric amplitudes of the incident, reflected, and transmitted waves over the respective basic polarization vectors. The coefficients of these expansions, which are found from Maxwell boundary conditions, determine the surface reflectivity for each incident-wave polarization, $r_{\omega,j}$. Then the total dimensionless emissivity equals $1 - \frac{1}{2}(r_{\omega,1} + r_{\omega,2})$.

The early works assumed that the ions are firmly fixed in the crystalline lattice. More recent works (van Adelsberg et al. 2005; Pérez-Azorín et al. 2005; Potekhin et al. 2012) consider not only this model, but also the opposite limit of free ions. The real reflectivity of the surface lies probably between the limits given by these two extreme models, but this problem is not yet definitely solved.
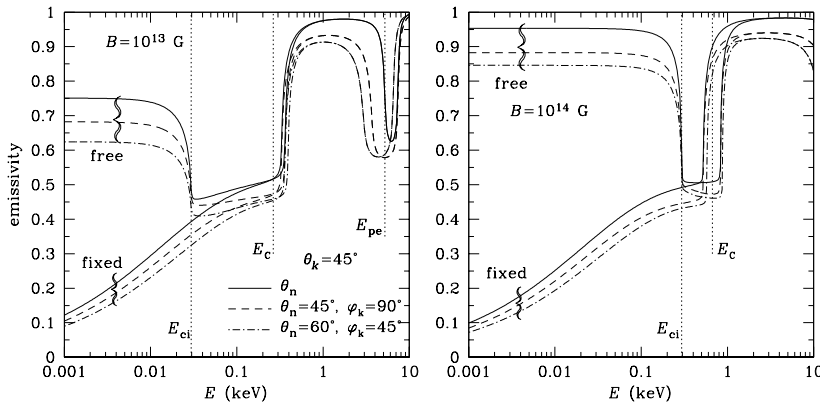
**Fig. 3** Dimensionless emissivity of a condensed iron surface at $B = 10^{13}$ G (*left panel*) and $10^{14}$ G (*right panel*), averaged over polarizations, is shown as a function of energy of a photon emitted at the angle $\theta_k = 45°$, for different magnetic-field inclination angles $\theta_n$ and azimuthal angles $\varphi_k$. For each parameter set, two curves are obtained in the models of free and fixed ions. Vertical dotted lines mark positions of the characteristic energies: the ion cyclotron energy $E_{ci} = \hbar\omega_{ci}$, the electron plasma energy $E_{pe} = \hbar\omega_{pe}$, and the hybrid energy $E_C$. The groups of curves marked "free" and "fixed" correspond to the models of free and fixed ions, mentioned in the text.

Figure 3 shows examples of the emissivity, normalized to the blackbody intensity, as a function of the photon energy $E = \hbar\omega$, in both the free- and fixed-ion limits, for the wave-vector inclination angle $\theta_k = 45°$, $B = 10^{13}$ G and $10^{14}$ G, and different values of the magnetic-field inclination $\theta_n$ and azimuthal angles $\varphi_k$. The characteristic energies $E_{ci} = \hbar\omega_{ci}$, $E_{pe} = \hbar\omega_{pe}$, and $E_C = E_{ci} + E_{pe}^2/\hbar\omega_c$ are marked. The spectral features near these energies are explained in van Adelsberg et al. (2005). For instance, the emissivity suppression at $E_{ci} \lesssim E \lesssim E_C$ is due to the strong damping of one of the two normal modes in the plasma in this energy range. There is a resonant absorption, depending on the directions of the incident wave and the magnetic field, near $E_{pe}$. The local flux density of radiation from a condensed surface is equal to the Planck function $\mathscr{B}_{\omega,T}$ multiplied by the normalized emissivity.

In Fig. 3, the emissivity is averaged over polarizations. But $r_{\omega,1} \neq r_{\omega,2}$, hence the thermal emission of a condensed surface is polarized, the polarization depending in a nontrivial way on the frequency $\omega$ and angles $\theta_n$, $\theta_k$, and $\varphi_k$. For example, the degree of linear polarization can reach tens percent near the frequencies $\omega_{ci}$ and $\omega_{pe}$, which makes promising the polarization diagnostics of NSs with condensed surfaces. The intensity and the polarization degree can be evaluated using analytical approximations for a condensed iron surface at $B = 10^{12} - 10^{14}$ G (Potekhin et al. 2012).

## 6.2 Thin and layered atmospheres

Motch et al. (2003) suggested that some NSs can possess a hydrogen atmosphere of a finite thickness above the solid iron surface. If the optical depth of such atmosphere is small for some wavelengths and large for other ones, this should lead to a pecu-

liar spectrum, different from the spectra of thick atmospheres. Ho et al. (2007) and Suleimanov et al. (2009, 2010b) calculated such spectra using simplified boundary conditions for the radiative transfer equation at the inner boundary of the atmosphere. More accurate boundary conditions (Potekhin et al. 2012) take into account that an extraordinary or ordinary wave, falling from the atmosphere on the surface, gives rise to reflected waves of both normal polarizations, whose intensities add to the respective intensities of the waves emitted by the condensed surface.

In general, local spectra of radiation emitted by thin hydrogen atmospheres over a condensed surface reveal a narrow absorption line corresponding to the proton cyclotron resonance in the atmosphere, features related to atomic transitions broadened by motion effects (Appendix A), and a kink corresponding to the ion cyclotron energy of the substrate ions. Some of these features may be absent, depending on the atmosphere thickness and magnetic field strength. At high energies, the spectrum is determined by the condensed-surface emission, which is softer than the spectrum of the thick hydrogen atmosphere.

The origin of the thin H atmospheres remains hazy. Ho et al. (2007) discussed three possible scenarios. First, it is the accretion from the interstellar medium. But its rate should be very low, in order to accumulate the hydrogen mass $4\pi R^2 y_{col} \sim 10^{-20} M_\odot$ in $\sim 10^6$ years. Another scenario assumes diffusive nuclear burning of a hydrogen layer accreted soon after the formation of the NS (Chiu and Salpeter 1964; Chang and Bildsten 2003). But this process is too fast at the early cooling epoch, when the star is relatively hot, and would have rapidly consumed all the hydrogen on the surface (Chiu and Salpeter 1964; Chang and Bildsten 2004). The third possibility is a self-regulating mechanism, driven by nuclear spallation in collisions with ultra-relativistic particles at the regions of open field lines (Jones 1978). An estimate of the penetration depth of the magnetospheric accelerated particles indicates that this process could create a hydrogen layer of the necessary thickness $y_{col} \sim 1$ g cm$^{-2}$ (Ho et al. 2007).

It is natural to consider also an atmosphere having a helium layer beneath the hydrogen layer. Indeed, all three scenarios assume that a hydrogen-helium mixture appears originally at the surface, and the strong gravity quickly separates these two elements. Such "sandwich atmosphere" was considered by Suleimanov et al. (2009), where the authors showed that its spectrum can have two or three absorption lines in the range $E \sim (0.2-1)$ keV at $B \sim 10^{14}$ G.

## 7 Modeling observed spectra

In order to apply the local spectra models described in Sects. 5 and 6 to observations, one has to calculate a synthetic spectrum, which would be observed at a large distance $D$ from the star. Such calculation should include the effects of General Relativity, which are significant.

The photon frequency, which equals $\omega$ in the local inertial reference frame, undergoes a redshift to a smaller frequency $\omega_\infty$ in the remote observer's reference frame. Therefore a thermal spectrum with effective temperature $T_{eff}$, measured by the remote

observer, corresponds to a lower effective temperature

$$T_{\text{eff}}^{\infty} = T_{\text{eff}}/(1+z_g),  \tag{34}$$

where $z_g \equiv \omega/\omega_{\infty} - 1 = (1-x_g)^{-1/2} - 1$ is the redshift parameter and the compactness parameter $x_g = 2GM/c^2R$ of a typical NS lies between 1/5 and 1/2. Here and hereafter the symbol $\infty$ indicates that the quantity is measured at a large distance from the star and can differ from its value near the surface.

Along with the radius $R$ that is determined by the equatorial length $2\pi R$ in the local reference frame, one often considers an *apparent radius* for a remote observer,

$$R_{\infty} = R(1+z_g).  \tag{35}$$

With decreasing $R$, $z_g$ increases so that the apparent radius has a minimum, $\min R_{\infty} \approx 12-14$ km (Haensel et al. 2007, Chapt. 6).

The apparent photon luminosity $L_{\text{ph}}^{\infty}$ and the luminosity in the stellar reference frame $L_{\text{ph}}$ are determined by the Stefan-Boltzmann law

$$L_{\text{ph}}^{\infty} = 4\pi\sigma_{\text{SB}}R_{\infty}^2 (T_{\text{eff}}^{\infty})^4, \quad L_{\text{ph}} = 4\pi\sigma_{\text{SB}}R^2T_{\text{eff}}^4  \tag{36}$$

with $\sigma_{\text{SB}} = \pi^2/(60\hbar^3c^2)$ and $T_{\text{eff}}^{\infty}$ in energy units. According to (34)–(35),

$$L_{\text{ph}}^{\infty} = (1-x_g)L_{\text{ph}} = L_{\text{ph}}/(1+z_g)^2.  \tag{37}$$

In the absence of spherical symmetry, it is convenient to define a local effective surface temperature $T_s$ by the relation $F_{\text{ph}}(\theta, \varphi) = \sigma_{\text{SB}}T_s^4$, where $F_{\text{ph}}$ is the local radial flux density at the surface point, determined by the polar angle ($\theta$) and azimuth ($\varphi$) in the spherical coordinate system. Then

$$L_{\text{ph}} = \int_0^{\pi} \sin\theta \, d\theta \int_0^{2\pi} d\varphi \, F_{\text{ph}}(\theta, \varphi).  \tag{38}$$

The same relation connects the apparent luminosity $L_{\text{ph}}^{\infty}$ (37) with the apparent flux $F_{\text{ph}}^{\infty} = \sigma_{\text{SB}}(T_s^{\infty})^4$ in the remote system, in accord with the relation $T_s^{\infty} = T_s/(1+z_g)$ analogous to (34).

The expressions (34), (35) and (37) agree with the GR concepts of light ray bending and time dilation near a massive body. If the angle between the wave vector $\boldsymbol{k}$ and the normal to the surface $\mathbf{n}$ at the emission point is $\theta_k$, then the observer receives a photon whose wave vector makes an angle $\theta > \theta_k$ with $\mathbf{n}$. The rigorous theory of the influence of the light bending near a star on its observed spectrum has been developed by Pechenick et al. (1983) and cast in a convenient form by Page (1995) and Pavlov and Zavlin (2000). Beloborodov (2002) suggested the simple approximation

$$\cos\theta_k = x_g + (1-x_g)\cos\theta,  \tag{39}$$

which is applicable at $x_g < 0.5$ with an error within a few percent. At $\cos\theta_k < x_g$, Eq. (39) gives $\theta > \pi/2$, which allows the observer to look behind the NS horizon.

Magnetic fields and temperatures of NSs vary from one surface point to another. In order to reproduce the radiation spectrum that comes to an observer, one can use
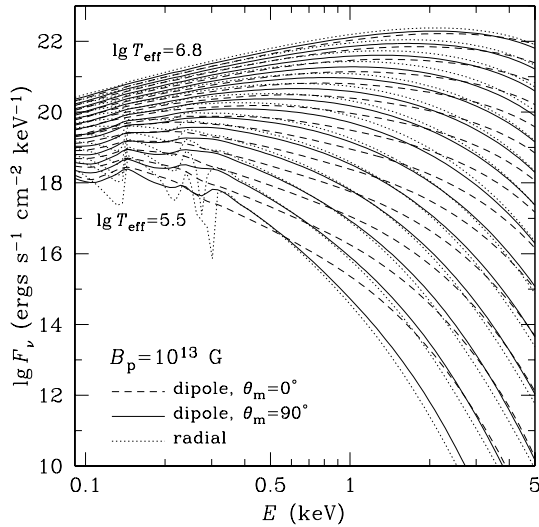
**Fig. 4** Integral spectra of a hydrogen atmosphere of a neutron star with $M = 1.4 M_\odot$, $R = 12$ km, and with different effective temperatures $T_{\text{eff}}$ ($\log T_{\text{eff}}$ (K) from 5.5 to 6.8 with step 0.1). The dashed and solid lines represent the model with a dipole field of strength $B_{\text{p}} = 10^{13}$ G at the pole and oriented along and across the line of sight, respectively. For comparison, the dotted curve shows the model with a constant field $B = 10^{13}$ G, normal to the surface.

the equations derived by Poutanen and Gierliński (2003) (see also Poutanen and Beloborodov 2006). In the particular case of a slowly rotating spherical star they give the following expression for spectral flux density related to the circular frequency $\omega_\infty = \omega \sqrt{1 - r_g/R}$ at a large distance $D$ from the star:

$$F_{\omega_\infty} = (1 - x_g)^{3/2} \frac{R^2}{D^2} \int I_\omega(\boldsymbol{k}; \theta, \varphi) \cos \theta_k \sin \theta \, \mathrm{d}\theta \, \mathrm{d}\varphi, \tag{40}$$

where the integration is performed under the condition $\cos \theta_k > 0$. The problem is complicated, because the surface distributions of the magnetic field and the temperature are not known in advance. A conventional fiducial model is the relativistic dipole (Ginzburg and Ozernoi 1965), while the temperature distribution, consistent with the magnetic-field distribution, is found from calculations of heat transport in NS envelopes considered by Page et al. in this volume.

For the model of partially ionized H atmospheres described in Sect. 5, synthetic spectra were calculated by Ho et al. (2008). Examples are shown in Fig. 4. We see that the spectral features are strongly smeared by the averaging over the surface, and the spectrum depends on the magnetic axis orientation $\theta_{\text{m}}$. When the star rotates, the latter dependence leads to the phase dependence of the spectra.

Such spectra of partially ionized, strongly magnetized NS atmospheres composed of hydrogen have been included in the package *XSPEC* (Arnaud 1996) under the names NSMAX and NSMAXG (see Ho 2014 and references therein).

## 8 Theory versus observations

Theoretical models of nonmagnetic atmospheres are successfully applied to analyses of spectra of many NSs with relatively weak magnetic fields $B \lesssim 10^9$ G. However, the nonmagnetic models are inadequate for the strongly magnetized NSs ($B \gg 10^9$ G). The theoretical framework for modeling the atmospheres of such stars is described above. As argued in Sect. 4, models of strongly magnetized NS atmospheres must take the bound species and their radiative transitions into account. Let us consider a few examples where models of magnetized, partially ionized atmospheres have been used to study their thermal radiation.

8.1 RX J1856.5–3754

In the case of RX J1856.5−3754, it is surprising the absence of absorption features and it is necessary to consider the spectrum in the X-ray and optical ranges simultaneously. The X-ray and optical spectra correspond to substantially different effective temperatures if fitted separately with blackbodies. To solve this problem, Ho et al. (2007) involved the model of a thin atmosphere described in Sect. 6.2. The measured spectrum of RX J1856.5−3754 was fitted in the entire range from X-rays to optical within observational errorbars. The best agreement between the theoretical and observed spectra has been achieved at the atmosphere column density $y_{col} = 1.2$ g cm$^{-2}$, $B \sim (3-4) \times 10^{12}$ G, $T_{eff}^{\infty} = (4.34 \pm 0.03) \times 10^5$ K, $z_g = 0.25 \pm 0.05$, and $R_{\infty} = 17.2^{+0.5}_{-0.1} D_{140}$ km. Here, the errors are given at the $1\sigma$ significance level, and $D_{140} \equiv D/(140 \text{ pc})$. Note that a fit of the observed X-ray spectrum with the Planck function yields a 70% higher temperature and a 3.5 times smaller radius of the emitting surface. Such huge difference exposes the importance of a correct physical interpretation of an observed spectrum for evaluation of NS parameters.

With the aid of expressions (34)−(35), we obtain from these estimates $T_{eff} = (5.4 \pm 1.1) \times 10^5$ K, $R = 13.8^{+0.9}_{-0.6} D_{140}$ km, and $M = 1.68^{+0.22}_{-0.15} D_{140} M_{\odot}$. Ho et al. (2007) adopted the value $D = 140$ pc from Kaplan et al. (2002). Using a recent update of the distance estimate, $D = 123^{+11}_{-15}$ pc (Walter et al. 2010), one obtains $R = 12.1^{+1.3}_{-1.6}$ km and $M = 1.48^{+0.16}_{-0.19} M_{\odot}$. Nevertheless, the given interpretation of the spectrum is somewhat questionable, since it does not agree with the magnetic-field estimate $B \approx 1.5 \times 10^{13}$ G, obtained for this star from timing analysis (van Kerkwijk and Kaplan 2008).

Using the same thin-atmosphere model, Ho (2007) analyzed the light curve of RX J1856.5−3754 and obtained constraints on the geometry of rotational and magnetic axes. It turned out that the light curve can be explained if one of these angles is small ($< 6°$), while the other angle lies between $20°$ and $45°$. In this case, the radio emission around the magnetic poles does not cross the line of sight. As noted by Ho (2007), this may explain the non-detection of this star as a radio pulsar (Kondratiev et al. 2009).

## 8.2 RX J1308.6+2127

Hambaryan et al. (2011) analyzed the X-ray spectrum of the X-ray source RX J1308.6+2127 (RBS 1223), which reveals a more complex structure than RX J1856.5 $-3754$. It can be described by a wide absorption line centered around $\hbar\omega = 0.3$ keV, superposed on the Planck spectrum, with the line parameters depending on the stellar rotation phase. Using all $2003-2007$ *XMM-Newton* observations of this star, the authors obtained a set of X-ray spectra for different rotation phases. They tried to interpret these spectra with different models, assuming magnetic fields $B \sim 10^{13} - 10^{14}$ G, different atmosphere compositions, possible presence of a condensed surface and a finite atmosphere.

As a result, the authors managed to describe the observed spectrum and its rotational phase dependence with the use of the model of an iron surface covered by a partially ionized hydrogen atmosphere with $y_{col} \sim 1-10$ g cm$^{-2}$, with mutually consistent asymmetric bipolar distributions of the magnetic field and the temperature, with the polar values $B_{p1} = B_{p2} = (0.86 \pm 0.02) \times 10^{14}$ G, $T_{p1} = 1.22^{+0.02}_{-0.05}$ MK, and $T_{p2} = 1.15 \pm 0.04$ MK. The magnetic field and temperature proved to be rather smoothly distributed over the surface. When compared to the theoretical model of Pérez-Azorin et al. (2006), such smooth distribution implies that the crust does not contain a superstrong toroidal magnetic field. The effective temperature is $T_{eff} \approx 0.7$ MK. The gravitational redshift is estimated to be $z_g = 0.16^{+0.03}_{-0.01}$, which converts into $(M/M_\odot)/R_6 = 0.87^{+0.13}_{0.05}$ and suggests a stiff EOS of the NS matter.

Note that the paper by Hambaryan et al. (2011) preceded that by Potekhin et al. (2012), where the treatment of the condensed surface and thin atmosphere was improved (Sect. 6). An analysis of the spectrum of RX J1308.6+2127 with the use of the improved results remains to be done in the future.

## 8.3 1E 1207.4−5209

The discovery of absorption lines in the spectrum of CCO 1E 1207.4−5209 at energies $E \sim 0.7N$ keV ($N = 1, 2, \ldots$) immediately entrained the natural assumption that they are caused by cyclotron harmonics (Bignami et al. 2003). As shown in Potekhin (2010), such harmonics can be only electronic, as the ion harmonics are unobservable. Therefore, this interpretation implies $B \approx 7 \times 10^{10}$ G. Mori et al. (2005) argued that only the first and second lines in the spectrum of 1E 1207.4−5209 are statistically significant, but some authors take also the third and fourth lines into account. This hypothesis was developed by Suleimanov et al. (2010a, 2012a), who considered two types of the electron cyclotron harmonics: the quantum oscillations of the Coulomb logarithm and the relativistic thermal harmonics (Sect. 5.5.2). An analogous explanation of the shape of the spectrum may possibly be applied also to CCO PSR J0821−4300 (Gotthelf et al. 2013).

Mori and Hailey (2006) have critically analyzed the earlier hypotheses about the origin of the absorption lines in the spectrum of 1E 1207.4−5209 and suggested their own explanation. They analyzed and rejected such interpretations as the lines of molecular hydrogen ions, helium ions, and also as the cyclotron lines and their

harmonics. One of the arguments against the latter interpretation is that the fundamental cyclotron line should have much larger depth in the atmosphere spectrum than actually observed. Another argument is that the cyclotron lines and harmonics have small widths at a fixed $B$, therefore their observed width in the integral spectrum is determined by the $B$ distribution. Thus the width of all lines should be the same, but observations do not confirm it. These arguments of Mori and Hailey (2006) were neglected by Suleimanov et al. (2010a, 2012a). Both groups of authors studied the cyclotron harmonics in spectra of fully ionized plasmas. This approach is indeed justified for the CCOs, because the impact of bound states on the spectra is small at $B \lesssim 10^{11}$ G and $T \gtrsim 10^6$ K (Potekhin, Chabrier, and Ho, in preparation).

As an alternative, Mori and Hailey (2006) and Mori and Ho (2007) suggested models of atmospheres composed of mid-$Z$ elements. The authors found that an oxygen atmosphere with magnetic field $B = 10^{12}$ G provides a spectrum similar to the observed one. However, the constraint $B < 3.3 \times 10^{11}$ G obtained by Halpern and Gotthelf (2010) disagrees with this model, but rather favors the electron-cyclotron interpretation of the lines.

Unlike the cases of RX J1856.5−3754 and RX J1308.6+2127 that were considered above, there is no published results of a detailed fitting of the observed spectrum of 1E 1207.4−5209 with a theoretical model. Thus all suggested explanations of the spectrum of this object remain hypothetical.

## 8.4 Rotation Powered Pulsars

### 8.4.1 PSR J1119−6127

Ng et al. (2012) applied the partially ionized, strongly magnetized hydrogen atmosphere model (Ho et al. 2008) to interpretation of observations of pulsar J1119−6127, for which the estimate based on spindown gives an atypically high field $B = 4 \times 10^{13}$ G. In the X-ray range, it emits pulsed radiation, which has apparently mostly thermal nature. At fixed $D = 8.4$ kpc and $R = 13$, the bolometric flux gives an estimate of the mean effective temperature $T_{\text{eff}} \approx 1.1$ MK. It was difficult to explain, however, the large pulsed fraction $(48 \pm 12\%)$ by the thermal emission. Ng et al. (2012) managed to reproduce the X-ray light curve of this pulsar assuming that one of its magnetic poles is surrounded by a heated area, which occupies 1/3 of the surface, is covered by hydrogen and heated to 1.5 MK, while the temperature of the opposite polar cap is below 0.9 MK.

### 8.4.2 PSR B0943+10

Storch et al. (2014) applied a similar analysis to interpretation of observations of pulsar B0943+10, which shows correlated radio and X-ray mode switches. The authors have taken $B = 2 \times 10^{12}$ G inferred from the pulsar spindown, assumed $M = 1.2 M_\odot$ and $R = 12$ km, and modeled the emitting area as a hot spot covered by a partially ionized hydrogen atmosphere. They found that an atmosphere with $T_{\text{eff}} \approx (1.4 - 1.5)$ MK and emission radius $R_{\text{em}} \approx 85$ m matches the radio-quiet X-ray spectrum, whereas

previous blackbody fits gave $T_{bb} = 3$ MK and $R_{bb} \approx 20 - 30$ m. The authors showed that the large X-ray pulse fraction observed during the radio quiet phase can be explained by including the beaming effect of a magnetic atmosphere, while remaining consistent with the dipole field geometry constrained by radio observations.

*8.4.3 PSR J0357+3205*

A middle-aged radio-quiet gamma-ray pulsar J0357+3205 was discovered in gamma-rays with Fermi and later in X-rays with Chandra and XMM-Newton observatories. It produces an unusual thermally-emitting pulsar wind nebula observed in X-rays. Kirichenko et al. (2014) fitted the spectrum of this pulsar with several different multicomponent models. In the physically realistic case where the incomplete ionization of the atmosphere was taken into account, they used the NSMAX model (Ho et al. 2008) for the thermal spectral component and a power-law model for the nonthermal one and fixed $M = 1.4 M_{\odot}$ and $B = 10^{12}$ G. They obtained an acceptable fit ($\chi^2 = 1.05/244$) with a very loose constraint on the radius, $R_{\infty} = 8^{+12}_{-5}(D/500 \text{ pc})$ km.

## 9 Conclusions

We have considered the main features of neutron-star atmospheres and radiating surfaces and outlined the current state of the theory of the formation of their spectra. The interpretation of observations enters a qualitatively new phase, free from the assumptions of a blackbody spectrum or the "canonical model" of neutron stars. Spectral features, compatible with absorption lines in some cases, have been discovered in thermal spectra of strongly magnetized neutron stars. On the agenda is their detailed theoretical description, which may provide information on the surface composition, temperature and magnetic field distributions. However, in order to disentangle these parameters, a number of problems related to the theory of magnetic atmospheres and radiating surfaces still have to be solved.

## A The effects of finite atomic masses

In this Appendix, we give a brief account of the effects of motion of atomic nuclei in strong magnetic fields on the quantum-mechanical characteristics of bound species and the ionization equilibrium of partially ionized plasmas (for a more detailed review, see Potekhin 2014)

### A.1 The finite-mass effects on properties of atoms

An atomic nucleus of finite mass, as any charged particle, undergoes oscillations in the plane (*xy*) perpendicular to **B**, which are quantized in the ion Landau levels. In an atom or a molecule, these oscillations are entangled with the electron motion. Therefore the longitudinal projections of the orbital moments of the electrons and the nucleus are not conserved separately. Different atomic quantum numbers correspond to

different oscillation energies of the atomic nucleus, multiple of its cyclotron energy $\hbar\omega_{ci}$. As a result, the energy of every level gets an addition, which is non-negligible if the magnetic parameter $\gamma$ is not small compared to the nucleus-to-electron mass ratio $m_i/m_e$.

For the hydrogen atom and hydrogenlike ions, a conserved quantity is $\hbar s$, which corresponds to the difference of longitudinal projections of orbital moments of the atomic nucleus and the electron, and the sum $N + s$ plays role of a nuclear Landau number, $N$ being the electron Landau number. For the bound states in strong magnetic fields, $N = 0$, therefore the nuclear oscillatory addition to the energy equals $s\hbar\omega_{ci}$. Thus the binding energy of a hydrogen atom at rest is

$$E_{sv} = E_{sv}^{(0)} - \hbar\omega_{ci}s, \tag{41}$$

where $E_{sv}^{(0)}$ is the binding energy in the approximation of non-moving nucleus. It follows that the values of $s$ are limited for the bound states. In particular, all bound states have $s = 0$ at $B > 6 \times 10^{13}$ G.

The account of the finite nuclear mass is more complicated for multielectron atoms. Al-Hujaj and Schmelcher (2003) have shown that the contribution of the nuclear motion to the binding energy of a non-moving atom equals $\hbar\omega_{ci}S(1 + \delta(\gamma))$, where $(-S)$ is the total magnetic quantum number of the atom, and $|\delta(\gamma)| \ll 1$.

The astrophysical simulations assume finite temperatures, hence thermal motion of particles. The theory of motion of a system of point charges in a constant magnetic field was reviewed by Johnson et al. (1983). The canonical momentum $\boldsymbol{P}$ is not conserved in a magnetic field. A relevant conserved quantity is pseudomomentum

$$\boldsymbol{K} = \boldsymbol{P} + \frac{1}{2c}\boldsymbol{B} \times \sum_i q_i \boldsymbol{r_i}. \tag{42}$$

If the system is electrically neutral as a whole, then all Cartesian components of $\boldsymbol{K}$ can be determined simultaneously (i.e., their quantum-mechanical operators commute with each other). For a charged system (an ion), one can determine $K^2$ simultaneously with either $K_x$ or $K_y$, but $K_x$ and $K_y$ do not commute. The specific effects related to collective motion of a system of charged particles are especially important in NS atmospheres at $\gamma \gg 1$. In particular, so called decentered states may become populated, where an electron is localized mostly in a "magnetic well" aside from the Coulomb center.

For a hydrogen atom, $\boldsymbol{K} = \boldsymbol{P} - (e/2c)\boldsymbol{B} \times \boldsymbol{r}$, where $\boldsymbol{r}$ connects the proton and the electron. Early studies of this particular case were done by Gor'kov and Dzyaloshinskiĭ (1968); Burkova et al. (1976); Ipatova et al. (1984). Numerical calculations of the energy spectrum of the hydrogen atom with an accurate treatment of the effects of motion across a strong magnetic field were performed by Vincke et al. (1992) and Potekhin (1994). Bound-bound radiative transitions of a moving H atom in a plasma were studied by Pavlov and Potekhin (1995), and bound-free transitions by Potekhin and Pavlov (1997).

Figure 5 shows the energies, oscillator strengths, and photoionization cross-sections of a hydrogen atom moving in a magnetic field with $\gamma = 1000$. The reference point is taken to be the sum of the zero-point oscillation energies of free electron and proton, $(\hbar\omega_c + \hbar\omega_{ci})/2$. Therefore the negative energies in Fig. 5 a correspond to bound states ($E_{sv} = -E > 0$). At small transverse pseudomomenta $K_\perp$, the energies of low levels in Fig. 5a exceed the binding energy of the field-free hydrogen atom (1 Ry) by an order of magnitude. However, the binding energy decreases with increasing $K_\perp$, and it can become negative for the states with $s \neq 0$ due to the term $\hbar\omega_{ci}s$ in Eq. (41). Such states are metastable. In essence, they are continuum resonances. Note that the transverse atomic velocity equals $\partial E/\partial \boldsymbol{K}$, therefore it attains a maximum at the inflection points ($K_\perp = K_c$) on the curves in Fig. 5a and decreases with further increase of $K_\perp$, while the average electron-proton distance continues to increase. At $K_\perp > K_c$ the atom goes into the decentered state, where the electron and proton are localized near their guiding centers, separated by distance $r_* = (a_B^2/\hbar)K_\perp/\gamma$.

Figure 5b shows oscillator strengths for the main transitions from the ground state to excited discrete levels. Since the atomic wave-functions are symmetric with respect to the $z$-inversion for the states with even $v$, and antisymmetric for odd $v$, only the transitions that change the parity of $v$ are allowed for the polarization along the field ($\alpha = 0$), and only those preserving the parity for the orthogonal polarizations ($\alpha = \pm1$). For the atom at rest, in the dipole approximation, due to the conservation of the $z$-projection of the total angular momentum of the system, absorption of a photon with polarization $\alpha = 0, \pm1$ results in the change of $s$ by $\alpha$. This selection rule for a non-moving atom manifests itself in vanishing oscillator strengths at $K_\perp \to 0$ for $s \neq \alpha$. In an appropriate coordinate system (Burkova et al. 1976; Potekhin 1994), the symmetry is restored at $K_\perp \to \infty$, therefore the transition with $s = \alpha$ is the only one that survives also in the limit of large pseudomomenta. But in the intermediate region of $K_\perp$, where the transverse atomic
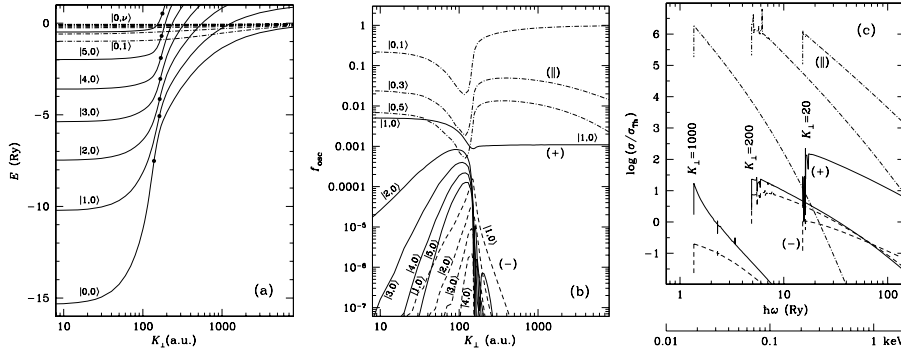
**Fig. 5** (a) energies, (b) oscillator strengths, and (c) photoionization cross-sections for a hydrogen atom moving across magnetic field $B = 2.35 \times 10^{12}$ G. Energies of states $|s,0\rangle$ (solid curves) and $|0,\nu\rangle$ (dot-dashed curves) are shown as functions of the transverse pseudomomentum $K_\perp$ (in atomic units). The heavy dots on the solid curves are the inflection points at $K_\perp = K_c$. The $K_\perp$-dependence of oscillator strengths (b) is shown for transitions from the ground state to the states $|s,0\rangle$ under influence of radiation with polarization $\alpha = +1$ (solid curves) and $\alpha = -1$ (dashed curves), and also for transitions into states $|0,\nu\rangle$ for $\alpha = 0$ (dot-dashed curves). Cross sections of photoionization (c) under the influence of radiation with $\alpha = +1$ (solid curves), $\alpha = -1$ (dashed curves), and $\alpha = 0$ (dot-dashed curves) are shown for the ground state as functions of the photon energy in Ry (the upper x-scale) and keV (the lower x-scale) at $K_\perp = 20$ a.u. (the right curve), $K_\perp = 200$ a.u. (the middle curve), and $K_\perp = 1000$ a.u. (the left curve of every type).

velocity is not small, the cylindrical symmetry is broken, so that transitions to other levels are allowed. Thus the corresponding oscillator strengths in Fig. 5b have maxima at $K_\perp \approx K_c$. Analytical approximations for these oscillator strengths, as well as for the dependences of the binding energies $E_{s\nu}(K_\perp)$, are given in Potekhin (1998).

Figure 5c shows photoionization cross-sections for hydrogen in the ground state as functions of photon energy at three values of $K_\perp$. The leftward shift of the ionization threshold with increasing $K_\perp$ corresponds to the decrease of the binding energy that is shown in Fig. 5a, while the peaks and dips on the curves are caused by resonances at transitions to metastable states $|s,\nu;K\rangle$ with positive energies (see Potekhin and Pavlov 1997, for a detailed discussion).

Quantum-mechanical calculations of the characteristics of the He$^+$ ion that moves in a strong magnetic field are performed by Bezchastnov et al. (1998); Pavlov and Bezchastnov (2005). The basic difference from the case of a neutral atom is that the ion motion is restricted by the field in the transverse plane, therefore the values of $K^2$ are quantized (Johnson et al. 1983). Clearly, the similarity relations for the ions with nonmoving nuclei (Sect. 4.2.1) do not hold anymore.

Currently there is no detailed calculation of binding energies, oscillator strengths, and photoionization cross-sections for atoms and ions other than H and He$^+$, arbitrarily moving in a strong magnetic field. For such species one usually neglects the decentered states and uses a perturbation theory with respect to $K_\perp$ (e.g., Mori and Hailey 2002; Medin et al. 2008). This approximation can be sufficient for simulations of relatively cool atmospheres of moderately magnetized NSs. A condition of applicability of the perturbation theory for an atom with mass $m_a = Am_u$ requires $T/E^{(0)} \ll m_a/(\gamma m_e) \approx 4A/B_{12}$ (Potekhin 2014). If $B \lesssim 10^{13}$ G and $T \lesssim 10^6$ K, it is satisfied for low-lying levels of carbon and heavier atoms.

## A.2 The finite-mass effects on the ionization equilibrium and thermodynamics

Since quantum-mechanical characteristics of an atom in a strong magnetic field depend on the transverse pseudomomentum $K_\perp$, the atomic distribution over $K_\perp$ cannot be written in a closed form, and only the distribution over longitudinal momenta $K_z$ remains Maxwellian. The first complete account of these effects has been taken in Potekhin et al. (1999) for hydrogen atmospheres. Let $p_{s\nu}(K_\perp) d^2 K_\perp$ be the probability

of finding a hydrogen atom in the state $|s, \nu\rangle$ in the element $d^2K_\perp$ near $\boldsymbol{K}_\perp$ in the plane of transverse pseudomomenta. Then the number of atoms in the element $d^3K$ of the pseudomomentum space equals

$$dN(\boldsymbol{K}) = N_{s\nu} \frac{\lambda_a}{2\pi\hbar} \exp\left(-\frac{K_z^2}{2m_a T}\right) p_{s\nu}(K_\perp) d^3K, \tag{43}$$

where $m_a$ is the mass of the atom, $\lambda_a = [2\pi\hbar^2/(m_a T)]^{1/2}$ is its thermal wavelength, and $N_{s\nu} = \int dN_{s\nu}(\boldsymbol{K})$ is the total number of atoms with given discrete quantum numbers. The distribution $N_{s\nu} p_{s\nu}(K_\perp)$ is not known in advance, but should be calculated in a self-consistent way by minimization of the free energy including the nonideal terms. It is convenient to define deviations from the Maxwell distribution with the use of generalized occupation probabilities $w_{s\nu}(K_\perp)$. Then the atomic contribution to the free energy equals (Potekhin et al. 1999)

$$F_{id}^{at} + F_{int}^{at} = T \sum_{s\nu} N_{s\nu} \int \ln\left[n_{s\nu} \lambda_a^3 \frac{w_{s\nu}(K_\perp)}{\exp(1)\mathscr{Z}_{s\nu}}\right] p_{s\nu}(K_\perp) d^2K_\perp, \tag{44}$$

where

$$\mathscr{Z}_{s\nu} = \frac{\lambda_a^2}{(2\pi\hbar^2)} \int_0^\infty w_{s\nu}(K_\perp) e^{E_{s\nu}(K_\perp)/T} K_\perp dK_\perp. \tag{45}$$

The nonideal part of the free energy that describes atom-atom and atom-ion interactions and is responsible for the pressure ionization has been calculated by Potekhin et al. (1999) with the use of the hard-sphere model. The plasma model included also hydrogen molecules $H_2$ and chains $H_n$, which become stable in the strong magnetic fields. For this purpose, approximate formulae of Lai (2001) have been used, which do not take full account of the motion effects, therefore the results of Potekhin et al. (1999) are reliable only when the molecular fraction is small.

This hydrogen-plasma model underlies thermodynamic calculations of hydrogen atmospheres of NSs with strong and superstrong magnetic fields (Potekhin and Chabrier 2003, 2004). Mori and Heyl (2007) applied the same approach with slight modifications to strongly magnetized helium plasmas. One of the modifications was the use of the plasma microfield distribution from Potekhin et al. (2002) for calculation of the $K_\perp$-dependent occupation probabilities. Mori and Heyl considered atomic and molecular helium states of different ionization degrees. Their treatment included rotovibrational molecular levels and the dependence of binding energies on orientation of the molecular axis relative to $\boldsymbol{B}$. The $K_\perp$-dependence of the energy, $E(K_\perp)$, was described by an analytical fit, based on an extrapolation of adiabatic calculations at small $K_\perp$. The effects of motion of atomic and molecular ions were not considered.

# References

A.A. Abdo, M. Ajello, A. Allafort, et al., Astrophys. J. Suppl. Ser. 208, 17 (2013)

S.L. Adler, Ann. Phys. (N.Y.) 67, 599 (1971)

D.N. Aguilera, J.A. Pons, J.A. Miralles, Astron. Astrophys. 486, 255 (2008)

O.-A. Al-Hujaj, P. Schmelcher, Phys. Rev. A 67, 023403 (2003)

K.A. Arnaud, *Astronomical Data Analysis Software and Systems V*, ed. by G. Jacoby, J. Barnes, ASP Conf. Ser. 101, 17 (1996); http://starchild.gsfc.nasa.gov/xanadu/xspec/

J.N. Bahcall, R.A. Wolf, Astrophys. J. 142, 1254 (1965)

A.M. Beloborodov, Astrophys. J. 566, L85 (2002)

V.S. Beskin, Ya.N. Istomin, A.A. Philippov, Phys. Usp. 56, 164 (2013)

V.G. Bezchastnov, G.G. Pavlov, J. Ventura, Phys. Rev. A 58, 180 (1998)

G.F. Bignami, P.A. Caraveo, A. De Luca, S. Mereghetti, Nature 423, 725 (2003)

G.S. Bisnovatyi-Kogan, Phys. Usp. 49, 53 (2006)

G.S. Bisnovatyi-Kogan, N.R. Ikhsanov, Astron. Rep. 58, 217 (2014)

S. Bogdanov, Astrophys. J. 762, 96 (2013)

K. Boshkaev, L. Izzo, J.A. Rueda, R. Ruffini, Astron. Astrophys. 555, A151 (2013)

W. Brinkmann, Astron. Astrophys. 82, 352 (1980)

W. Brinkmann, H. Ögelman, Astron. Astrophys. 182, 71 (1987)

E.F. Brown, L. Bildsten, R.E. Rutledge, Astrophys. J. 504, L95 (1998)

T. Bulik, G.G. Pavlov, Astrophys. J. 469, 373 (1996)

S. Burke-Spolaor, in *Proceedings of IAUS 291 "Neutron Stars and Pulsars: Challenges and Opportunities after 80 years"*, ed. by J. van Leeuwen. Cambridge University Press, Cambridge (2014) p. 95

L.A. Burkova, I.E. Dzyaloshinskiĭ, G.P. Drukarev, B.S. Monozon, Sov. Phys. JETP 44, 276 (1976)

P.A. Caraveo, A. De Luca, M. Marelli, et al., Astrophys. J. 725, L6 (2010)

P. Chang, L. Bildsten, Astrophys. J. 585, 464 (2003)

P. Chang, L. Bildsten, Astrophys. J. 605, 830 (2004)

A.F. Cheng, D.J. Helfand, Astrophys. J. 271, 271 (1983)

H.-Y. Chiu, E.E. Salpeter, Phys. Rev. Lett. 12, 413 (1964)

R. Cohen, J. Lodenquai, M. Ruderman, Phys. Rev. Lett. 25, 467 (1970)

A. De Luca, in *40 Years of Pulsars: Millisecond Pulsars, Magnetars and More*, ed. by C. Bassa, Z. Wang, A. Cumming, V.M. Kaspi. AIP Conf. Proc. 983, 311 (2008)

A. De Luca, P. Caraveo, S. Mereghetti, M. Negroni, G.F. Bignami, Astrophys. J. 623, 1051 (2005)

A. De Luca, R.P. Mignani, A. Sartori, et al., Astron. Astrophys. 525, 106 (2011)

T. Detmer, P. Schmelcher, L.S. Cederbaum, Phys. Rev. A 57, 1767 (1998)

R.C. Duncan, C. Thompson, Astrophys. J. 392, L9 (1992)

W. Ebeling, G. Norman, J. Stat. Phys. 110, 861 (2003)

E. Fermi, Z. f. Physik 26, 54 (1924)

B.T. Gänsicke, T.M. Braje, R.M. Romani, Astron. Astrophys. 386, 1001 (2002)

R.H. Garstang, Rep. Prog. Phys. 40, 105 (1977)

F.P. Gavriil, V.M. Kaspi, P.M. Woods, Nature 419, 142 (2002)

F.P. Gavriil, M.E. Gonzalez, E.V. Gotthelf, V.M. Kaspi, M.A. Livingstone, P.M. Woods, Science 319, 1802 (2008)

V.L. Ginzburg, *The Propagation of Electromagnetic Waves in Plasmas* (2nd ed.). Pergamon, London (1970)

V.L. Ginzburg, L.M. Ozernoi, Sov. Phys. JETP 20, 689 (1965)

Yu.N. Gnedin, G.G. Pavlov, Sov. Phys. JETP 38, 903 (1974)

Yu.N. Gnedin, R.A. Sunyaev, Astron. Astrophys. 36, 379 (1974)

L.P. Gor'kov, I.E. Dzyaloshinskiĭ, Sov. Phys. JETP 26, 449 (1968)

E.V. Gotthelf, J.P. Halpern, J. Alford, Astrophys. J. 765, 58 (2013)

C.B. Haakonsen, M.L. Turner, N.A. Tacik, R.E. Rutledge, Astrophys. J. 749, 52 (2012); https://github.com/McPHAC/

F. Haberl, Astrophys. Space Sci. 308, 181 (2007)

P. Haensel, A.Y. Potekhin, D.G. Yakovlev, *Neutron Stars 1: Equation of State and Structure*. Springer, New York (2007)

L.K. Haines, D.H. Roberts, Am. J. Phys. 37, 1145 (1969)

J.P. Halpern, E.V. Gotthelf, Astrophys. J. 709, 436 (2010)

V. Hambaryan, R. Neuhäuser, F. Haberl, M.M. Hohle, A.D. Schwope, Astron. Astrophys. 497, L9 (2009)

V. Hambaryan, V. Suleimanov, A.D. Schwope, et al., Astron. Astrophys. 534, A74 (2011)

A.K. Harding, D. Lai, Rep. Prog. Phys. 69, 2631 (2006)

C.O. Heinke, G.B. Rybicki, R. Narayan, J.E. Grindlay, Astrophys. J. 644, 1090 (2006)

A. Hewish, S.J. Bell, J.D.H. Pilkington, P.F. Scott, R.A. Collins, Nature 217, 709 (1968)

J.S. Heyl, L. Hernquist, Phys. Rev. D 55, 2449 (1997)

J.S. Heyl, N.J. Shaviv, Phys. Rev. D 66, 023002 (2002)

W.C.G. Ho, Mon. Not. R. astron. Soc. 380, 71 (2007)

W.C.G. Ho, in *Magnetic Fields Throughout Stellar Evolution (Proc. IAU Symp. 302)*, ed. by M. Jardine, P. Petit, H.C. Spruit. Cambridge University Press, Cambridge (2014) p. 435

W.C.G. Ho, C.O. Heinke, Nature 462, 71 (2009)

W.C.G. Ho, D. Lai, Mon. Not. R. astron. Soc. 338, 233 (2003)

W.C.G. Ho, D.L. Kaplan, P. Chang, M. van Adelsberg, A.Y. Potekhin, Mon. Not. R. astron. Soc. 375, 821 (2007)

W.C.G. Ho, A.Y. Potekhin, G. Chabrier, Astrophys. J. Suppl. Ser. 178, 102 (2008)

M.M. Hohle, F. Haberl, J. Vink, et al., Mon. Not. R. astron. Soc. 423, 1194 (2012)

I.P. Ipatova, A.Yu. Maslov, A.V. Subashiev, Sov. Phys. JETP 60, 1037 (1984)

N. Itoh, Mon. Not. R. astron. Soc. 173, 1P (1975)

M.V. Ivanov, P. Schmelcher, Phys. Rev. A 61, 022505 (2000)

P. Jones, Mon. Not. R. astron. Soc. 184, 807 (1978)

B.R. Johnson, J.O. Hirschfelder, K.H. Yang, Rev. Mod. Phys. 55, 109 (1983)

B.B. Kadomtsev, Sov. Phys. JETP 31, 945 (1970)

B.B. Kadomtsev, V.S. Kudryavtsev, JETP Lett. 13, 42 (1971)

A.D. Kaminker, G.G. Pavlov, Yu.A. Shibanov, Astrophys. Space Sci. 86, 249 (1982)

D.L. Kaplan, M.H. van Kerkwijk, Astrophys. J. 705, 798 (2009)

D.L. Kaplan, M.H. van Kerkwijk, J. Anderson, Astrophys. J. 571, 447 (2002)

D.L. Kaplan, A. Kamble, M.H. van Kerkwijk, W.C.G. Ho, Astrophys. J. 736, 117 (2011)

U. Kappes, P. Schmelcher, Phys. Rev. A 54, 1313 (1996)

V.M. Kaspi, PNAS 107, 7147 (2010)

V. K. Khersonskii, Sov. Astron. 31, 646 (1987)

A. Kirichenko, A. Danilenko, Yu. Shibanov, et al., Astron. Astrophys. 564, A81 (2014)

K. Kohri, S. Yamada, Phys. Rev. D 65, 043006 (2002)

V.I. Kondratiev, M.A. McLaughlin, M. Burgay, et al., Astrophys. J. 702, 692 (2009); erratum: ibid. 708, 910 (2010)

A. Kubo, J. Phys. Chem. A 111, 5572 (2007)

D. Lai, Rev. Mod. Phys. 73, 629 (2001)

D. Lai, W.C.G. Ho, Astrophys. J. 566, 373 (2002)

R. Lenzen, J. Trümper, Nature 271, 216 (1978)

E.H. Lieb, J.P. Solovej, J. Yngvason, Phys. Rev. Lett. 69, 749 (1992)

M.A. Livingstone, C.-Y. Ng, V.M. Kaspi, F.P. Gavriil, E.V. Gotthelf, Astrophys. J. 730, 66 (2011)

V.M. Malofeev, O.I. Malov, D.A. Teplykh, Astrophys. Space Sci. 308, 211 (2007)

I.F. Malov, Astron. Rep. 54, 925 (2010)

R.N. Manchester, G.B. Hobbs, A. Teoh, M. Hobbs, Astron. J. 129, 1993 (2005)

M. Marelli, A. De Luca, P.A. Caraveo, Astrophys. J. 733, 82 (2011)

M.A. McLaughlin, A.G. Lyne, D.R. Lorimer, et al., Nature 439, 817 (2006)

Z. Medin, D. Lai, Phys. Rev. A 74, 062507 (2006a)

Z. Medin, D. Lai, Phys. Rev. A 74, 062508 (2006b)

Z. Medin, D. Lai, Mon. Not. R. astron. Soc. 382, 1833 (2007)

Z. Medin, D. Lai, A.Y. Potekhin, Mon. Not. R. astron. Soc. 383, 161 (2008)

S. Mereghetti, A&AR 15, 225 (2008)

S. Mereghetti, Braz. J. Phys. 43, 35 (2013)

P. Mészáros *High-Energy Radiation from Magnetized Neutron Stars*. University of Chicago Press, Chicago (1992)

J.J. Miller, M.A. McLaughlin, N. Rea, et al., Astrophys. J. 776, 104 (2011)

M.C. Miller, Mon. Not. R. astron. Soc. 255, 129 (1992)

M.C. Miller, D. Neuhauser, Mon. Not. R. astron. Soc. 253, 107 (1991)

K. Mori, C.J. Hailey, Astrophys. J. 564, 914 (2002)

K. Mori, C.J. Hailey, Astrophys. J. 648, 1139 (2006)

K. Mori, J. Heyl, Mon. Not. R. astron. Soc. 376, 895 (2007)

K. Mori, W.C.G. Ho, Mon. Not. R. astron. Soc. 377, 905 (2007)

K. Mori, J.C. Chonko, C.J. Hailey, Astrophys. J. 631, 1082 (2005)

C. Motch, V.E. Zavlin, F. Haberl, Astron. Astrophys. 408, 323 (2003)

C.-Y. Ng, P.O. Slane, B.M. Gaensler, J.P. Hughes, Astrophys. J. 686, 508 (2008)

C.-Y. Ng, V.M. Kaspi, in *Astrophysics of neutron stars 2010: A Conference in Honor of M. Ali Alpar*, ed. by E. Göğüş, T. Belloni, Ü. Ertan. AIP Conf. Proc. 1379, 60 (2011)

C.-Y. Ng, V.M. Kaspi, W.C.G. Ho, et al., Astrophys. J. 761, 65 (2012)

S.A. Olausen, V.M. Kaspi, Astrophys. J. Suppl. Ser. 212, 6 (2014)

D. Page, Astrophys. J. 442, 273 (1995)

G.G. Pavlov, V.G. Bezchastnov, Astrophys. J. 635, L61 (2005)

G.G. Pavlov, Yu.N. Gnedin, Sov. Sci. Rev. E: Astrophys. Space Phys. 3, 197 (1984)

G.G. Pavlov, A.N. Panov, Sov. Phys. JETP 44, 300 (1976)

G.G. Pavlov, A.Y. Potekhin, Astrophys. J. 450, 883 (1995)

G.G. Pavlov, V.E. Zavlin, Astrophys. J. 529, 1011 (2000)

G.G. Pavlov, Yu.A. Shibanov, D.G. Yakovlev, Astrophys. Space Sci. 73, 33 (1980)

G.G. Pavlov, Yu.A. Shibanov, V.E. Zavlin, R.D. Meyer, in *The Lives of the Neutron Stars*, NATO *ASI* Series C vol. 450, ed. by M.A. Alpar, Ü. Kiziloğlu, and J. van Paradijs. Kluwer, Dordrecht (1995) p. 71.

K.R. Pechenick, C. Ftaclas, J.M. Cohen, Astrophys. J. 274, 846 (1983)

J.F. Pérez-Azorín, J.A. Miralles, J.A. Pons, Mon. Not. R. astron. Soc. 433, 275 (2005)

J.F. Pérez-Azorín, J.A. Miralles, J.A. Pons, Astron. Astrophys. 451, 1009 (2006)

J.A. Pons, F.M. Walter, J.M. Lattimer, et al., Astrophys. J. 564, 981 (2002)

J.A. Pons, J.A. Miralles, U. Geppert, Astron. Astrophys. 496, 207 (2009)

S.B. Popov, J.A. Pons, J.A. Miralles, P.A. Boldin, B. Posselt, Mon. Not. R. astron. Soc. 401, 2675 (2010)

A.Y. Potekhin, J. Phys. B: At. Mol. Opt. Phys. 27, 1073 (1994)

A.Y. Potekhin, Phys. Plasm. 3, 4156 (1996)

A.Y. Potekhin, J. Phys. B: At. Mol. Opt. Phys. 31, 49 (1998)

A.Y. Potekhin, Astron. Astrophys. 518, A24 (2010)

A.Y. Potekhin, Phys. Usp. 57, no. 8, in press (2014); arXiv:1403.0074

A.Y. Potekhin, G. Chabrier, Astrophys. J. 585, 955 (2003)

A.Y. Potekhin, G. Chabrier, Astrophys. J. 600, 317 (2004)

A.Y. Potekhin, G. Chabrier, Astron. Astrophys. 550, A43 (2013)

A.Y. Potekhin, D. Lai, Mon. Not. R. astron. Soc. 376, 793 (2007)

A.Y. Potekhin, G.G. Pavlov, Astrophys. J. 483, 414 (1997)

A.Y. Potekhin, G.G. Pavlov, J. Ventura, Astron. Astrophys. 317, 618 (1997)

A.Y. Potekhin, G. Chabrier, Yu.A. Shibanov, Phys. Rev. E 60, 2193 (1999); erratum:
    *ibid.* **63** 019901 (2000)

A.Y. Potekhin, D. Gilles, G. Chabrier, Phys. Rev. E 65, 036412 (2002)

A.Y. Potekhin, D. Lai, G. Chabrier, W.C.G. Ho, Astrophys. J. 612, 1034 (2004)

A.Y. Potekhin, V.F. Suleimanov, M. van Adelsberg, K. Werner, Astron. Astrophys.
    546, A121 (2012)

J. Poutanen, A.M. Beloborodov, Mon. Not. R. astron. Soc. 373, 836 (2006)

J. Poutanen, M. Gierliński, Mon. Not. R. astron. Soc. 343, 1301 (2003)

M. Rajagopal, R. Romani, Astrophys. J. 461, 327 (1996)

M. Rajagopal, R. Romani, M.C. Miller, Astrophys. J. 479, 347 (1997)

N. Rea, P. Esposito, in *High-Energy Emission from Pulsars and their Systems*, ed. by
    N. Rea, D.F. Torres. Springer, Berlin (2011) p. 247

Ö.E. Rögnvaldsson, I. Fushiki, E.H. Gudmundsson, C.J. Pethick, J. Yngvason, As-
    trophys. J. 416, 276 (1993)

R.W. Romani, Astrophys. J. 313, 718 (1987)

H. Ruder, G. Wunner, H. Herold, F. Geyer, *Atoms in Strong Magnetic Fields*.
    Springer, Berlin (1994)

M.A. Ruderman, Phys. Rev. Lett. 27, 1306 (1971)

E.E. Salpeter, Astrophys. J. 134, 669 (1961)

P. Schmelcher, T. Detmer, L.S. Cederbaum, Phys. Rev. A 64, 023410 (2001)

N. Shabaltas, D. Lai, Astrophys. J. 748, 148 (2012)

V.D. Shafranov, in *Reviews of Plasma Physics*, vol. 3, ed. by M.A. Leontovich, Con-
    sultants Bureau, New York (1967) p. 1

Yu.A. Shibanov, V.E. Zavlin, Astron. Lett. 21, 3 (1995)

Yu.A. Shibanov, G.G. Pavlov, V.E. Zavlin, J. Ventura, Astron. Astrophys. 266, 313
    (1992)

A.A. Sokolov, I.M. Ternov, *Radiation from Relativistic Electrons*. Am. Inst. Phys.,
    New York (1986)

A. Spitkovsky, Astrophys. J. 648, 51 (2006)

N.I. Storch, W.C.G. Ho, D. Lai, S. Bogdanov, C.O. Heinke, Astrophys. J. 789, L27
    (2014)

T. Strohmayer, L. Bildsten, in *Compact Stellar X-Ray Sources*, ed. by W.H.G. Lewin,
    M. van der Klis. Cambridge University Press, Cambridge (2006) p. 113

V. Suleimanov, A.Y. Potekhin, K. Werner, Astron. Astrophys. 500, 891 (2009)

V.F. Suleimanov, G.G. Pavlov, K. Werner, Astrophys. J. 714, 630 (2010a)

V. Suleimanov, V. Hambaryan, A.Y. Potekhin, et al., Astron. Astrophys. 522, A111 (2010b)

V. Suleimanov, J. Poutanen, M. Revnivtsev, K. Werner, Astrophys. J. 742, 122 (2011)

V.F. Suleimanov, G.G. Pavlov, K. Werner, Astrophys. J. 751, 15 (2012a)

V. Suleimanov, J. Poutanen, K. Werner, Astron. Astrophys. 545, A120 (2012b)

V.F. Suleimanov, D. Klochkov, G.G. Pavlov, K. Werner, Astrophys. J. Suppl. Ser. 210, 13 (2014)

G.L. Surmelian, R.F. O'Connel, Astrophys. J. 190, 741 (1974); erratum: Astrophys. J. 204, 311 (1976)

D. Teplykh, A. Rodin, V. Malofeev, S. Logvinenko, in *Radio Pulsars: An Astrophysical Key to Unlock the Secrets of the Universe*, ed. by M. Burgay, N. D'Amico, P. Esposito, A. Pellizzoni, and A. Possenti. AIP Conf. Proc. 1357, 201 (2011)

N. Tetzlaff, T. Eisenbeiss, R. Neuhäuser, M.M. Hohle, Mon. Not. R. astron. Soc. 417, 617 (2011)

A. Thorolfsson, Ö.E. Rögnvaldsson, J. Yngvason, E.H. Gudmundsson, Astrophys. J. 502, 847 (1998)

J. Trümper, K. Denneri, N.D. Kylafis, Ü. Ertan, A. Zezas, Astrophys. J. 764, 49 (2013)

A.V. Turbiner, Astrophys. Space Sci. 308, 267 (2007)

A.V. Turbiner, J.C. López Vieyra, N.L. Guevara, Phys. Rev. A 81, 042503 (2010)

R. Turolla, in *Neutron Stars and Pulsars*, ed. by W. Becker. Springer, Berlin (2009) p. 141

R. Turolla, P. Esposito, Int. J. Mod. Phys. 22, 1330024 (2013)

R. Turolla, S. Zane, J.J. Drake, Astrophys. J. 603, 265 (2004)

M. van Adelsberg, D. Lai, Mon. Not. R. astron. Soc. 373, 1495 (2006)

M. van Adelsberg, R. Perna, Mon. Not. R. astron. Soc. 399, 1523 (2009)

M. van Adelsberg, D. Lai, A.Y. Potekhin, P. Arras, Astrophys. J. 628, 902 (2005)

M.H. van Kerkwijk, D.L. Kaplan, Astrophys. J. 673, L163 (2008)

J. Ventura, Phys. Rev. D 19, 1684 (1979)

D. Viganò, J.A. Pons, Mon. Not. R. astron. Soc. 425, 248 (2012)

D. Viganò, N. Rea, J.A. Pons, D.N. Aguilera, J.A. Miralles, Mon. Not. R. astron. Soc. 434, 123 (2013)

D. Viganò, R. Perna, N. Rea, J.A. Pons, Mon. Not. R. astron. Soc. 443, 31 (2014)

M. Vincke, M. Le Dourneuf, D. Baye, J. Phys. B 25, 2787 (1992)

F.M. Walter, T. Eisenbeiß, J.M. Lattimer, et al., Astrophys. J. 724, 669 (2010)

G. Wunner, H. Ryder, W. Schmitt, H. Herold, Mon. Not. R. astron. Soc. 198, 769 (1982)

V.E. Zavlin, in *Neutron Stars and Pulsars*, ed. by W. Becker. Springer, New York (2009) p. 181

S. Zane, R. Turolla, L. Stella, A. Treves, Astrophys. J. 560, 384 (2001)

V.E. Zavlin, G.G. Pavlov, Yu.A. Shibanov, J. Ventura, Astron. Astrophys. 297, 441 (1995)

V.E. Zavlin, G.G. Pavlov, Astrophys. J. 616, 452 (2004)

V.E. Zavlin, G.G. Pavlov, Yu.A. Shibanov, Astron. Astrophys. 315, 141 (1996)

V.V. Zheleznyakov, *Radiation in Astrophysical Plasmas*. Kluwer, Dordrecht (1996)

F. Zwicky, Astrophys. J. 88, 522 (1938)